Electronic Structure and Magneto-Structural Correlations Study of Cu2UL Trinuclear Schiff Base Complexes: A 3d-5f-3d Case

Samir Meskaldji, Lotfi Belkhiri, Rémi Maurice, Karine Costuas, Boris Le Guennic, Abdou Boucekkine, Michel Ephritikhine

Electronic structure and magneto-structural correlations study of Cu_2UL trinuclear Schiff base complexes: a 3d-5f-3d case.

Samir Meskaldji,[a,b] Lotfi Belkhiri,[a,c*] Rémi Maurice,[d] Karine Costuas,[d] Boris Le Guennic,[d] Abdou Boucekkine,[d*] and Michel Ephritikhine[e]

[a] Laboratoire de Physique Mathématique et Subatomique LPMS, Département de Chimie, Université des Frères Mentouri, 25017 Constantine, Algeria.
[b] Ecole Normale Supérieure de l'Enseignement Technologique ENSET, 21000 Skikda, Algeria
[c] Centre de Recherche en Sciences Pharmaceutiques CRSP, Ali Mendjeli, 25000 Constantine, Algeria
[d] Univ Rennes, ISCR UMR 6226 CNRS, Campus de Beaulieu, 35042 Rennes Cedex, France.
[e] NIMBE, CEA, CNRS, Université Paris-Saclay, CEA Saclay, 91191 Gif-sur-Yvette, France.

Abstract:

The magnetic properties of trinuclear Schiff base complexes M_2AnL^i (M^{II} = Zn, Cu; An^{IV} = Th, U; L^i = Schiff base; i = 1-4,6,7,9), exhibiting the $[M(\mu\text{-}O)_2]_2U$ core structure with adjacent M1---U and M2---U and next-adjacent M1---M2 interactions, featuring 3d-5f-3d subsystems, have been investigated theoretically using relativistic ZORA/B3LYP computations combined with the broken symmetry (BS) approach. Bond order and natural population analyses reveal that the covalent contribution to the bonding within the Cu–O–U coordination is important thus favouring superexchange coupling between the transition metal and the uranium magnetic centers. The calculated coupling constants J_{CuU} between the Cu and U atoms, agree with the observed shift from the antiferromagnetic (AF) character of the $L^{1,2,3,4}$ complexes to the ferromagnetic (Ferro) of the $L^{6,7,9}$ ones. The structural parameters, *i.e.* the Cu---U distances and the Cu-O-U angles, as well as the electronic factors driving the magnetic couplings are discussed. The analyses are supported by the study of the mixed $ZnCuUL^i$ and Cu_2ThL^i systems, where in the first complex the Cu^{II} ($3d^9$) ion is replaced by the diamagnetic Zn^{II} ($3d^{10}$) one, whereas in the second complex the U^{IV} ($5f^2$) paramagnetic center is replaced by the diamagnetic Th^{IV} ($5f^0$) one.

Keywords: 3d-5f complexes; Schiff-based ligands; magneto-structural properties; super-exchange; DFT.

Corresponding Authors:

*Email (A. Boucekkine): abdou.boucekkine@univ-rennes1.fr
*Email (L. Belkhiri): lotfi.belkhiri@umc.edu.dz

Introduction:

Since the discovery of ferromagnetic interactions in trinuclear Cu_2Gd complexes in 1985 [1,2], the heterometallic 3d–4f complexes have attracted intense attention, both from experimental and theoretical sides, due to their many unique and specific potential applications in catalysis, magnetic cooling materials, luminescence, and notably as high spin molecules which could behave as single-molecule magnets (SMM) [3–8]. In particular, the combination of 3d and 4f elements to form large cluster aggregates has produced several novel SMMs with attractive blocking temperatures and thus a slow relaxation of magnetization [9-11]. Besides its fundamental aspects, the exchange coupling between a 4f ion and a spin carrier, a 3d ion or an organic radical has been studied with the aim of working out an accurate theoretical description as an effective magnetic interaction [12-21]. However, it seems difficult to envision high-nuclearity lanthanide clusters with concerted spin behavior [22-25]. The poor overlap of the contracted lanthanide 4f orbitals with bridging ligand orbitals, mostly results in weak magnetic exchange coupling [8, 25, 26].

In contrast, the larger spatial extent of the actinide 5f orbitals, relative to the 4f ones [26, 27] could favor stronger exchange couplings with 3d transition metals, resulting in larger antiferromagnetic (AF) or ferromagnetic (Ferro) couplings. However, molecular compounds containing $3d^n$ transition metal and $5f^n$ actinide ions are rare [26, 28, 29], and to date there are only few cases of mixed 3d-5f molecules for which a magnetic coupling constant has been measured [26, 29, 30-38]. Notably, evidence of such exchange coupling was nicely reviewed in 2009 by J. D. Rinehart *et al*. [26] for trinuclear transition metal-uranium systems. As reported by S.A. Kozimor *et al*. [36, 37] regarding the magnetic properties of the trinuclear pyrazolate-bridged MU_2 clusters of formula (cyclam)$M[(\mu\text{-}Cl)U^{IV}(Me_2Pz)_4]_2$ (M^{II} = Co, Ni, Cu, Zn; cyclam = 1,4,8,11-tetraazacyclotetradecane; Me_2Pz^- = 3,5-dimethylpyrazolate), a strong Ferro coupling with 15 $cm^{-1} < J < 48$ cm^{-1} is observed for the Co^{II}-containing species (NB: -2J convention) [36, 37]. To understand the origin of the Ferro coupling in this chloro-bridged $Co^{II}(\mu\text{-}Cl)U^{IV}$ complex, DFT calculations performed on the CoU_2 cluster revealed the unpaired electrons of the U^{IV} center to reside in the $5f_{xyz}$ and $5f_{z(x^2-y^2)}$ orbitals [36, 37]. The latter have δ symmetry with respect to the U–Cl bond, so that the overlap with σ and π orbitals of the chloride bridge will be zero.

This is arising from the strict orthogonality between the different bridging orbitals atoms, and any spin interaction from the Co^{II} $3d_z^2$ orbital throughout the chloride bridging ligands will lead to a Ferro exchange interaction [36]. Consistently, the Ferro exchange is also observed for the Ni_2U cluster, which features a S=1 Ni^{II} center, revealing a weaker Ni---U coupling constant (2.8 $cm^{-1} < J < 19\ cm^{-1}$) than for the Co---U congener [26, 36].

In addition, M. J. Monreal et *al*. [38] reported in 2007 the mixed-valence linear trinuclear ferrocenylamido $[Fe_2U\{C_5H_4NSi\text{-}(tBu)Me_2\}_4]^{0/+}$ cluster, which exhibits U---Fe distances of 2.9556(5) and 2.9686(5) Å, suggesting that magnetic coupling may occur through direct metal-metal Fe---U---Fe orbital overlap. Indeed, variable-temperature magnetic moment measurements show very different magnetic behavior for the mixed-valence $Fe^{II}U^{IV}Fe^{II}$ and $Fe^{II}U^{IV}Fe^{III}$ clusters. In the case of the latter cluster, the authors noted that the observed U^{IV}–Fe^{III} exchange is indicative of a weak Ferro interaction [38].

It is noteworthy that the observed exchange metal-uranium coupling constant magnitude, more than 15 cm^{-1}, shows that the exchange interaction between uranium and a transition metal ion can be stronger than for the lanthanide-transition metal analogs (typically $J < 4\ cm^{-1}$) [8, 26]. These characteristics may be due to the greater radial extension of the 5f valence orbitals of actinides than that of the 4f ones of their lanthanides congeners, providing increased overlap with bridging ligand orbitals, thereby enhancing the superexchange between bridged metal centers within a single core unit [26, 29].

To date, the most comprehensively studied class of 3d-5f uranium-transition metal assemblies exhibiting magnetic exchange interactions is the remarkable series of trinuclear complexes of general formula $[\{L^iM(py)_x\}_2An^{IV}]$ (An^{II} = Th, U; M^{II} = Co, Ni, Cu, Zn; L^i i = 1-9 Schiff base; x = 0-2), synthesized by Ephritikhine and coworkers in the early 2000s [30-34]. In this series, the bridging ligand L^i is a Schiff base, each presenting a modified diimino-hydrocarbon backbone. All are built up by two L-M units bound to the central actinide ion by two pairs of oxygen atoms, leading to $[M(\mu\text{–}O_b)_2]_2An$ cores, as shown on Scheme 1. Note that the corresponding O-U-O bond angles are nearly 90° (orthogonal U-O bonds) or 180° (*trans* U-O bonds).

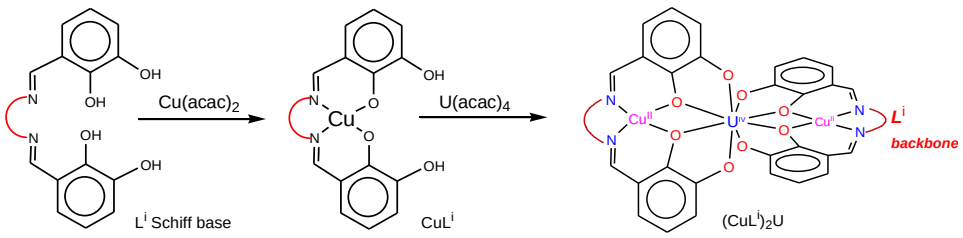

Scheme 1: Synthesis route to the $[\{L^iCu\}_2U^{IV}]$ complexes [30-33]

The first trinuclear systems were reported in 2000 with the formula $[\{L^7M(py)\}_2An^{IV}]$ (An^{IV} = Th, U; M^{II} = Co, Ni, Cu, Zn) with the hexadentate Schiff ligand L^7 = *N,N'*-bis(3-hydroxysalicylidene)-2,2-dimethyl-1,3-propanediamine}[30-33]. The X-ray structures of these systems show that the three metals M---U---M are linearly arranged. It is noteworthy that all the studied species, i.e., Co_2U, Ni_2U, Zn_2U, Cu_2U, and Cu_2Th species, are isostructural with a pseudo-symmetry (D_{2d}) broken by the pyridine coordination to the transition metal [33]. Moreover, the coordination environment of the uranium ion is practically the same in all complexes. Following the synthesis of the L^7 complexes, synthesis and X-ray structures of new hexadentate Schiff bases L^i = *N,N'*-bis(3-hydroxysalicylidene)-**R** ligands (i = 1-6, 8 and 9 ; R backbones) have been reported [34]. The different backbones are labelled as follows: R = 1,2-ethanediamine (**L**$^{\mathbf{1}}$), 2-methyl-1,2-propanediamine (**L**$^{\mathbf{2}}$), 1,2-cyclohexanediamine (**L**$^{\mathbf{3}}$), 1,2-phenylenediamine (**L**$^{\mathbf{4}}$), 4,5-dimethyl-1,2-phenylenediamine (**L**$^{\mathbf{5}}$), 1,3-propanediamine (**L**$^{\mathbf{6}}$), 2-amino-benzylamine (**L**$^{\mathbf{8}}$), and 1,4-butanediamine (**L**$^{\mathbf{9}}$) [34]. For the sake of simpler comparisons, we retain the previously used i indices (these were notably used in the work of Rinehart *et al.* [26]).

The analysis of the magnetic behaviors of these trinuclear $[\{L^iCu(py)_x\}_2U]$ complexes, revealed that the Cu^{II}---U^{IV} interactions within the L^i (i = 1-5) bases is AF, whereas it is Ferro for the L^i (i = 6-9) cases with two weakly or non-interacting Cu^{II}---Cu^{II} next-nearest neighbors [33, 34]. In this series of complexes, the shift from the AF to the Ferro character is related to an increase in the Cu---U distance associated to the lengthening in the diimino chain. This increase of the Cu---U separation is observed on the available four X-ray structures of the $UL^i_2Cu_2(py)$ complexes (i = 2, 6, 7, and 9), for which the average Cu---U distances are 3.538, 3.661, 3.641, and 3.647 Å, respectively [34]. Although the variable-temperature magnetic susceptibility data led to the qualitative determination of the sign of the exchange constant (Ferro J > 0 and AF coupling J < 0 for a *minus* sign convention), no attempts to quantify the magnitude of the

interaction have been done [30-34]. However, more recently, the application of the subtraction method, aiming at removing the contribution of the angular momentum of the U^{IV} center, to these trinuclear $UL^{i}_{2}Cu_{2}(py)$ systems by Rinehart et al. [26], gave $\Delta\chi_{M}T$ vs T plots confirming a shift of an AF to the Ferro coupling between the central U^{IV} ion and the paramagnetic Cu^{II} ions according to the ligand nature. The fitting of the magnetic data notably permitted to estimate lower bounds J_{min} for the exchange Cu^{II}---U^{IV} coupling strengths (in other words, estimates for the lower bounds for the absolute values of J, the J sign being well determined in the process). Indeed, the results afford two bounds for the exchange constants of J_{min} = 2.6 cm^{-1} and –1.8 cm^{-1} respectively for the L^{6} and L^{3} species, confirming the shift from the AF to the Ferro behavior [26].

Understanding the exchange interactions in polynuclear 3d-5f complexes is not only essential to the development of new models rationalizing the electronic structure and magnetic properties of such species but also may open the way to the design of actinide-based SMMs.

In this work, we aim to investigate the electronic structure and the nature of the magnetic interactions of the trinuclear $[\{L^{i}M^{II}(py)_{x}\}_{2}An^{IV}]$ (i = 1-9; M^{II} = Cu, Zn: An^{IV} = Th, U; x = 0-2) complexes exhibiting symmetrical $[Cu(\mu–O_{b})_{2}]_{2}An$ bridging cores, with $3d^{9}$-$5f^{2}$-$3d^{9}$ configurations [34]. The target backbones considered in this work, are shown on Scheme 2.

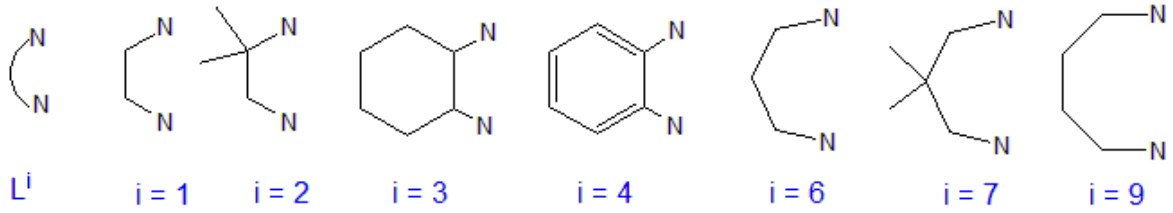

Scheme 2: Schematic representation of the diimino hydrocarbon backbones (L^{i}).

The dependence of the exchange coupling on structural parameters, namely the $Cu_{2}O_{4}U$ core geometry i.e., the Cu^{II}---U^{IV} distances and the Cu–O–U or O_{b}–Cu–O_{b} angles will be investigated. Such investigations have been successfully used previously in the case of the dioxo bimetallic $[UO_{2}(methanate)_{2}K]_{2}$ model system considering the $U_{2}(\mu–O_{b})_{2}$ diamond-shaped core distortion, revealing dramatic effects of small variation of the Cu–O–U angle on the strength and nature of the magnetic Cu^{II}---U^{IV} coupling [39,40]. Furthermore, the influence of the coordination environment of the metals on the magnetic properties will be explored by considering the mixed $ZnCuUL^{i}$ and $Cu_{2}ThL^{i}$ model systems, where the one Cu^{II} ($3d^{9}$) and U^{IV}

($5f^2$) paramagnetic centers are replaced by diamagnetic Zn^{II} ($3d^{10}$) and Th^{IV} (f^0) ones, respectively.

1. Computational details

All calculations were performed with the Amsterdam Density Functional (ADF) program, a part of the Amsterdam Molecular Simulation package (AMS2021.107 release) [41,42]. Relativistic corrections have been introduced via the zeroth-order regular approximation (ZORA) [43,44] accounting for essential scalar relativistic effects. In all cases, the starting molecular structures for the geometry optimizations are derived from the structures of the Cu_2UL complexes in the reported X-ray data [33, 34]. Two approaches have been applied, first the full geometry optimization of the whole Cu_2UL complexes and secondly by fixing the $[Cu(\mu–O_b)_2]_2U$ core geometries. The DFT geometry optimizations of the High Spin (HS) states, which have been carried out using the BP86 functional of Becke and Perdew [45, 46], employed triple-ζ-plus polarization (TZP) all-electron Slater type orbitals (STO) basis sets. Our previous recent works [29, 39, 40, 47-50], and several other theoretical studies [51, 52] have shown that such a ZORA/BP86/TZP procedure reproduces the experimental geometries of f-element compounds with a satisfying accuracy. As recommended [29, 53-57], the computation of the J exchange coupling constant has been done using the standard B3LYP hybrid functional [58, 59]. The B3LYP HS energies were obtained performing a single point calculation using the BP86 optimized geometries. The Broken Symmetry (BS) [60, 61] states were computed from the Molecular Orbitals (MOs) of the HS structures as starting guesses using the spin-flip recipe available in the ADF program [42].

The DFT/BS approach based on the hybrid functional B3LYP turns out to be reliable for a satisfying estimation of the coupling constants, not only for binuclear transition metal complexes [62-64], but also for actinide-containing molecules [29, 39, 40, 47-50, 54, 55,57], even though the use of the DFT single-determinant approach is a subject of debate [53, 65-69]. Note that alternatively, the PBE0 functional has also been used to compute the coupling between an actinide (Pu^{VI}) and a radical [70] (it is known that hybrid functionals usually lead to better values of coupling constants).

Comparative computations using the X-ray geometries of the complexes were also carried out. As usual, the hydrogen atoms coordinates have been optimized since they have not been located accurately with the available X-ray measurements.

Molecular structure drawings, spin densities and molecular orbital plots were generated using the ADF-GUI auxiliary program [42]. Finally, in the calculation, the ADF integration accuracy parameter, i.e., the grid numerical quality was set as high as 10^{-6} eV (numerical accuracy keyword "good").

a. Evaluation of the exchange coupling

The magnetic interaction between two atomic spins is usually described by the Heisenberg-Dirac-van Vleck (HDvV) Hamiltonian, as given by (-J convention):

$$\widehat{\mathcal{H}} = -J_{AB}\hat{S}_A\hat{S}_B \qquad (1)$$

where J_{AB} is the coupling constant between the A and B magnetic sites with total spin operators $\hat{S}_A$ and $\hat{S}_B$. A positive sign of the coupling constant J(cm^{-1}) indicates a Ferro interaction (parallel alignment of spins), whereas the negative sign indicates an AF interaction (anti parallel alignment of spins).

As reported by previous studies on polynuclear transition metal complexes [15,71], the Heisenberg Hamiltonian equation (1) can be extended to calculate the exchange coupling constants of polynuclear complexes by just expressing the difference in energy between different spin configurations as a sum of pairwise interactions.

For the trinuclear $L^iCuUCuL^i$ complexes considered here, the spin coupling model includes exchange interactions between adjacent metal centers, J_{12} and J_{23}, and the coupling between the terminal transition metal centers, J_{13}, as shown on scheme 3.

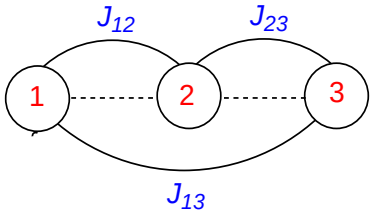

Scheme 3: different exchange coupling interactions

The resulting Hamiltonian, obtained by summing all the bicentric terms, is given by equation 2:

$$\hat{\mathcal{H}} = -J_{12}\hat{S}_1\hat{S}_2 - J_{23}\hat{S}_2\hat{S}_3 - J_{13}\hat{S}_1\hat{S}_3 \qquad (2)$$

Considering $S_1 = S_3 = ½$ for the Cu^{II} (d^9) metal centers and $S_2 = 1$ for the U^{IV} ($5f^2$) center, four non-equivalent spin configurations obtained by parallel and/or anti parallel alignments of the adjacent spins are obtained (see Scheme 4). The HS state has an $M_S = 2$ value, two intermediate-spin BS1 and BS2 configurations have $M_S = 1$ values and finally the low-spin BS configuration has an $M_S = 0$ value [71].

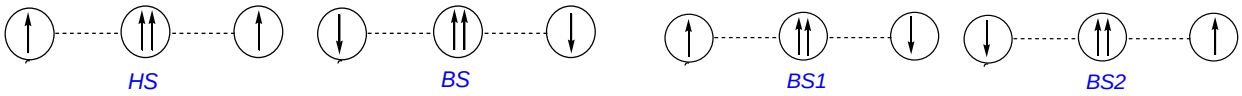

Scheme 4: spin state configurations

The relative energies of these four configurations can be explicitly written in terms of the coupling constants J_{12}, J_{23} and J_{13}, using the equation 2 and scheme 4 (we do a mapping of the computed energies onto the diagonal elements of the HDvV Hamiltonian, or in other words we extract the Ising coupling constants).

After fixing the zero of energy to the mean energy of the four computed configurations [69]:

$$E_o = \frac{E_{HS}+E_{BS}+E_{BS1}+E_{BS2}}{4} \qquad (3)$$

the energies of the four HS, BS1, BS2 and BS configurations are expressed as follows:

$$E_{HS} = E_o - J_{12}/2 - J_{23}/2 - J_{13}/4 \qquad (4)$$

$$E_{BS1} = E_o - J_{12}/2 + J_{23}/2 + J_{13}/4 \qquad (5)$$

$$E_{BS2} = E_o + J_{12}/2 - J_{23}/2 + J_{13}/4 \qquad (6)$$

$$E_{BS} = E_o + J_{12}/2 + J_{23}/2 - J_{13}/4 \qquad (7)$$

The combination of (4) + (5) leads to:

$$J_{12} = 2E_o - (E_{HS} + E_{BS1}) \qquad (8)$$

Then, (4) + (6) leads to:

$J_{23} = 2E_o - (E_{HS} + E_{BS2})$ (9)

Finally, (4) + (7) leads to:

$J_{13} = 4E_o - 2(E_{HS} + E_{BS})$ (10)

noting that $E_{BS} - E_{HS} = J_{12} + J_{23}$.

For the $L^iCuUCuL^i$ systems considered here, the BS1, BS2, and BS energies have been computed by performing a single point calculation using the molecular orbitals (MOs) of the HS structure as starting guess, and changing the spin on the corresponding metal center as said above, and finally reaching the self-consistent field convergence. It must be kept in mind that the evaluation of the coupling constant J derives from energy differences often smaller than ~0.5 kcal/mol (*i.e.*, ~170 cm^{-1}) [72] so that a very good accuracy of the calculations must be insured in order to avoid numerical round up errors.

Finally, for the mixed $L^iZnUCuL^i$ model complexes, exhibiting only two magnetic centers Cu(II)---U(IV) with the electronic configuration $3d^9$---$5f^2$, the Zn(II) center being diamagnetic (d^{10}), the formula of Yamaguchi et al. [73,74] could be used for the evaluation of the coupling constant J.

The corresponding expression is:

$$J_{12} = \frac{E_{BS} - E_{HS}}{\langle S^2 \rangle_{HS} - \langle S^2 \rangle_{BS}} \quad (11)$$

where $\langle S^2 \rangle_{HS}$ and $\langle S^2 \rangle_{BS}$ are the HS and BS mean values of the squared spin operator, respectively. This formula should be valid over the full range of coupling strengths, from the weak to the strong overlap limit [74,75,76]. Note that in our case, no deviation is expected from the Ising coupling constant (weak-coupling scheme).

Such ZnUCu model complexes were successfully used to calculate the coupling constants independently, by replacing one of the Ni^{II} ions by Zn^{II} in the mixed trinuclear Ni^{II}-Gd^{III}-Ni^{II} systems [71].

2. Results and Discussion

2.1. Geometry optimizations

We started our investigations by optimizing the geometries of the Schiff bases complexes $[\{L^iM^{II}(py)_x\}_2An^{IV}]$ (i = 1-9; M^{II} = Cu, Zn: An^{IV} = Th, U; x = 0-2) for which X-ray structures are available (in fact, we exclude the L^i = 5, 8 cases, for which we cannot perform a complete structural analysis by lack of any relevant experimental structure). For the $L^iCuUCuL^i$ complexes, whatever the number of pyridine molecules, the starting molecular structures for the geometries optimizations are derived from the L^i (i = 2,6,7,9) X-ray data [33,34]. Concerning the L^1, L^3 and L^4 systems, no experimental structural parameters are available in the literature and their molecular geometries are derived from the X-ray data of their $L^iZnUZnL^i$ (i = 1, 4) congeners. However, as no $L^3ZnUZnL^3$ X-ray data is available the structure of the Cu_2UL^3 model system has been fully optimized based on the $L^4ZnUZnL^4$ X-ray data [34]. The full geometry optimization that we previously carried out on diuranium systems [39,40], showed that small deviations between the X-ray and the fully optimized structures (*vide supra*) could be of tremendous importance for the magnetic property under consideration. For instance, it was observed in the case of the dihydroxo dichromium(III) system that a slight distortion of the $Cr_2(\mu\text{-}OH)_2$ magnetic core, results on large deviation of the magnetic behaviour [62]. Furthermore, replacing the DFT geometry by the X-ray one led to a better agreement between the computed and the observed magnetic coupling constant [29]. Consequently, for the analysis of the magnetic properties of the trinuclear $L^iCuUCuL^i$ species, it seems also crucial to consider the case of X-ray Cu_2O_4U core geometry fixed. This approach turned out to be fruitful relatively to the consideration of the fully optimized structures when investigating magnetic characters of uranium complexes [39,40].

First, let us consider the structures of the $L^iCuUCuL^i$ (i = 1–4, 6, 7, 9) complexes obtained from the ZORA/BP86/TZP geometry optimizations, displayed on Figure 1 along with the most relevant structural parameters of the magnetic core depicted on Figure 2.

ANTIFERROMAGNETIC SPECIES

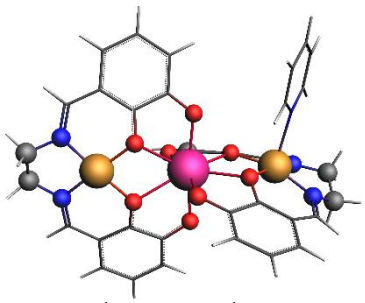

$L^1CuUCuL^1pyr$

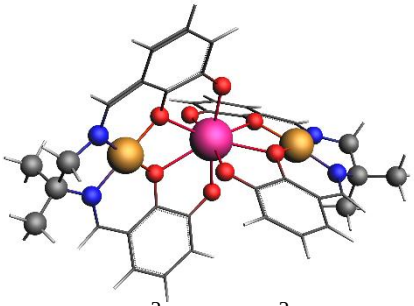

$L^2CuUCuL^2$

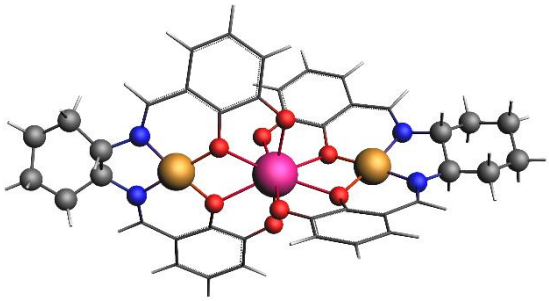

$L^3CuUCuL^3$

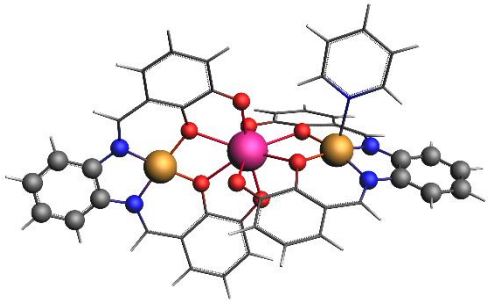

$L^4CuUCuL^4pyr$

FERROMAGNETIC SPECIES

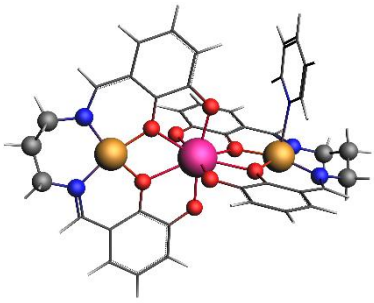

$L^6CuUCuL^6pyr$

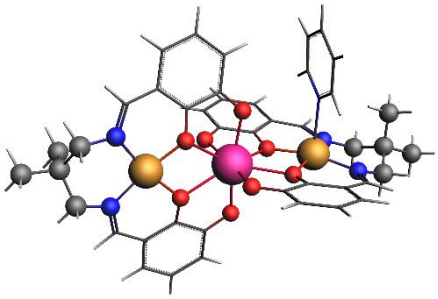

$L^7CuUCuL^7pyr$

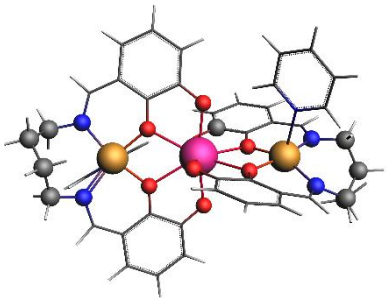

$L^9CupyrUCuL^9pyr$

Figure 1: Representation of the optimized molecular structures of the $L^iCuUCuL^i$ complexes. Pink, yellow, red and blue balls are used for emphasizing uranium, cupper, oxygen and nitrogen atoms, respectively.

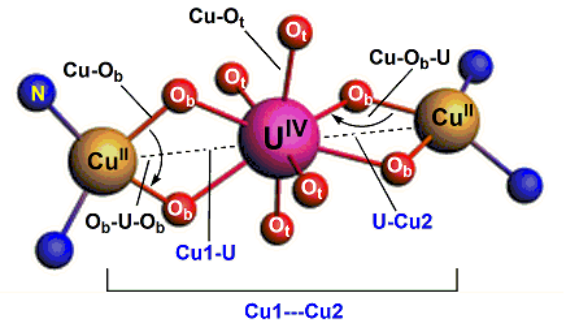

Figure 2: geometrical parameters of the Cu_2UO_8 core

In Table 1 we report the optimized metal–uranium Cu1---U/U---Cu2 distances and the average <Cu–O_b>, <Cu–O_t> bond distances (Å) as well as the interatomic Cu---Cu distance. The average <Cu1–O_b–U> and <Cu2–O_b–U> bond angles (°) for both sides are also reported as well as the Cu--U--Cu angle for the $L^iCuUCuL^i$ complexes in their HS state.

The considered Cu_2O_4U core is the X-ray one for the $L^iCuUCuL^i$ (i = 2,6,7,9) complexes and a modelled one for $L^iCuUCuL^i$ (i = 1,3,4) from their Zn congeners geometries. The fully optimized $L^iCuUCuL^i$ (i = 1,3,4) model geometries, which are derived from the $L^iZnUZnL^i$ (i = 1,3,4) congeners, are in line of the available observed experimental X-ray trends, especially with the lengthening of the Cu—U and Cu---Cu (Å) distances, when passing from the AF $L^2CuUCuL^2$ to the Ferro $L^iCuUCuL^i$ (i = 6,7,9) species [33, 34]. Furthermore, the <Cu1-O_b-U> and <Cu2-O_b-U> bond angles are well described by the DFT optimizations. Notably, the <Cu–O_b–U> bond angles (°) for the $L^iCuUCuL^i$ (i = 1,2,3,4) species, described as AF systems, are computed to be lower than those exhibited by their $L^{6,7,9}$ Ferro congeners.

Table 1: Relevant ZORA/BP86/TZP optimized (<average>) bond distances (Å) and angles (°) for the $Cu_2UL^i(pyr)_x$ (L^i = Shiff Bases) complexes in their quintet HS state (S = 2). See Figure 2 for the definition of the geometrical parameters. Available X-ray data are in bold.

$Cu_2UL^i(pyr)_x$	Cu_2L^1Upyr	Cu_2L^2U	Cu_2L^3U	Cu_2L^4Upyr	Cu_2L^6Upyr	Cu_2L^7Upyr	$Cu_2UL^9pyr_2$
Cu1-U/U-Cu2	3.560/3.561	**3.536/3.540**	3.555/3.558	3.573/3.580	**3.648/3.671**	**3.634/3.648**	**3.653/3.661**

<Cu1–O_b>	1.865	**1.865(2)**	1.898	1.900	**1.951(6)**	**1.950(6)**	**1.937(6)**
<Cu2–O_b>	1.981	**1.864(10)**	1.897	1.925	**1.917(7)**	**1.918(6)**	**1.952(6)**
<U–O_b>	2.468	**2.42(2)**	2.466	2.463	**2.45(2)**	**2.46(1)**	**2.447(2)**
<U–O_t>	2.336	**2.33(2)**	2.291	2.274	**2.30(2)**	**2.29(3)**	**2.298(14)**
<Cu1-O_b-U>	107.95	**111.05**	108.15	108.95	**111.91**	**111.51**	**112.35**
<Cu2-O_b-U>	108.05	**108.25**	108.81	108.94	**113.05**	**112.32**	**112.11**
Cu--U--Cu	173.0	**173.62(5)**	164.3	173.6	**175.92(3)** **174.98(4)**	**177.27(3)**	**178.51(3)**
Cu---Cu	7.108	**7.081**	7.102	7.123	**7.314**	**7.279**	**7.314**

The shift from AF to Ferro coupling occurs as the backbone of the Schiff base increases from two carbon atoms (i = 1-5) to three (i = 6-8) or four C atoms (i = 9) which are associated with a lengthening of the Cu---U distance [34]. However, it should be noted that this observation is only true for the four L^iCuUCuL^i (i = 2, 6, 7, and 9) complexes, for which the average X-ray Cu---U distances are 3.538, 3.661, 3.641, and 3.647 Å, respectively [34].

Table 1 also shows that the Cu---U bond distances are found shorter (below 3.6 Å) in L^iCuUCuL^i (i = 1,2,3,4) AF species than in the Ferro L^iCuUCuL^i (i = 6,7,9) ones (above 3.6 Å). It is also worth noting the slightly longer Cu2---U distance compared to the Cu1---U one and the smaller Cu–O_b–U bridging angles computed for the AF species in comparison to those obtained for the Ferro species. Finally, it appears that the main significant structural differences are caused by changing the length of the diimino backbone chain of the Schiff base L^i ligand, which induces the distortion of the Cu(μ–O_b)$_2$U bridging cores, in particular, the Cu–O_b–U angles or the Cu---U distance.

Regarding the L^iCuUCuL^i (i = 2,6,7,9) species, the Cu---U distance undergoes an average shortening from 3.657, 3.641, or 3.661 to 3.538 Å for e.g., L^9, L^7, or L^6 to L^2, respectively, correlating well with the increase of the O_b–Cu–O_b angle or decrease of the Cu–O_b–U one.

Moreover, the U–O_b (bridging) bond lengths range from 2.422 to 2.455(6) Å with an average of 2.43(3) Å, while the U–O_t (terminal) bond lengths range from 2.271(9) to 2.325(7) Å and average 2.30(3) Å [34]. These distances are slightly longer in the M_2Th thorium complexes, with averages distances 2.48(8) and 2.38(1) Å for Th–O_b and Th–O_t, respectively, consistent with the difference in the ionic radii of Th^{4+}(1.05 Å) and U^{4+} (1.00 Å) [34]. It can be seen also that the dihedral angle Cu–O_b–U–O_b is equal to 0.0°, indicating the perfect geometry planarity of the two perpendicular [Cu(μ–O_b)$_2$]$_2$U cores (Figure 2).

2.2. Electronic structure analyses.

To study the electronic structures and the natures of the metal-ligand bonding in the L^iCuUCuL^i complexes, natural population analyses (NPA) [77], Mayer [78], and Nalewajski-Mrozek (NM) [79,80] bond order analyses were performed at the optimized ZORA/B3LYP/TZP equilibrium geometries. The NPA approach is a better alternative to Mulliken population analysis [81] (MPA) for investigating the covalence in f-element complexes, yielding results that better agree with the experimental trends [82]. The computed net natural atomic charges (q), Mayer, and NM bond orders are given in Table 2.

The results of Table 2 show that the computed NPA charges on the uranium atom are *ca*. +1.73, which is much smaller than the formal value of +4 in U(IV), while values of *ca*. +1.40 are obtained for the Cu(II) metal ions (*vs.* +2 for the formal charge). Deviation to formal charges is generally attributed to the ligand-to-metal donation, the actual values themselves being also influenced by the arbitrary choice of a charge model. Covalent contributions to bonding may arise in the case of a favorable energy matching between the bridging ligand orbitals and the metal d/f orbitals [83-86]. This is not only important for the π oxo-network ligand, but might also favor superexchange coupling interactions within the [Cu(μ-O_b)$_2$]$_2$U core [33,34].

Table 2: ZORA/B3LYP/TZP NPA atomic spin density (ρ) and net charges (q), Mayer and NM average <Cu–O_b> and <U–O_b> bond orders of the L^iCuUCuL^i complexes in their HS and BS states. O_b are the bridging oxygen atoms (see Figure 2).

	NPA		Bond Order			
L^iCuUCuL^i(pyr)$_x$	Cu1/U/Cu2		<Cu–O_b>		<U–O_b>	
	ρ	q	Mayer	NM	Mayer	NM

$L^1CuUCuL^1pyr$	HS	0.59/2.04/0.63	+1.38/+1.72/+1.43	0.430	0.839	0.128	1.136
	BS	-0.58/2.01/-0.59	+1.37/+1.71/+1.39	0.416	0.827	0.179	1.166
$L^2CuUCuL^2$	HS	0.59/2.09/0.59	+1.38/+1.74/+1.38	0.436	0.847	0.168	1.138
	BS	-0.58/2.03/-0.58	+1.38/+1.75/+1.38	0.426	0.850	0.179	1.151
$L^3CuUCuL^3$	HS	0.59/2.04/0.59	+1.38/+1.73/+1.39	0.444	0.844	0.159	1.145
	BS	-0.58/2.03/-0.59	+1.38/+1.70/+1.39	0.420	0.827	0.176	1.168
$L^4CuUCuL^4pyr$	HS	0.59/2.03/0.63	+1.39/+1.70/+1.43	0.419	0.836	0.168	1.119
	BS	-0.59/2.03/-0.63	+1.38/+1.67/+1.43	0.402	0.825	0.185	1.143
$L^6CuUCuL^6pyr$	HS	0.64/2.04/0.61	+1.39/+1.73/+1.43	0.429	0.833	0.148	1.130
	BS	-0.60/2.03/-0.63	+1.39/+1.74/+1.42	0.418	0.850	0.181	1.170
$L^7CuUCuL^7$	HS	0.64/2.04/0.61	+1.39/+1.72/+1.43	0.438	0.834	0.144	1.132
	BS	-0.60/2.03/-0.60	+1.38/+1.73/+1.39	0.423	0.841	0.169	1.162
$L^9CuUCuL^9pyr_2$	HS	0.64/2.04/0.64	+1.43/+1.75/+1.43	0.439	0.830	0.146	1.152
	BS	-0.64/2.03/-0.64	+1.43/+1.73/+1.45	0.417	0.845	0.179	1.174

As previously observed in diuranium dioxo systems [39,40], the covalent bonds between oxygen atoms and uranium or copper centers, as described by the Mayer bond orders, could lead to a significant electronic communication that favors Cu---U metal-metal super-exchange couplings. Moreover, the NM approach, which accounts for both ionic and covalent contributions, gives greater Cu–O/O–U bond orders than Mayer's ones, noting that the NM O-U bond order is higher than the Cu-O one. The Cu_2O_4U cores exhibit formally Cu–O and U–O single bond characters, in opposite to the previously studied dioxo diamond core U_2O_2 diuranium(V) complex which exhibits both single and double U–O bonds [39,40]. Moreover, these results reveal that the Cu–O_b bonds feature more pronounced covalent character than their O_b–U congeners, as shown by the significantly greater Mayer bond orders. It is noteworthy that the Mayer Cu–O_b bond orders are found lower for the BS than the HS one, while they increase for the BS O_b–U ones. The same trend is predicted for the NM bond orders as they increase significantly for the O_b–U bond when passing from the HS to the BS state. This latter result seems to be due to the larger polarization effects with the more localized $5f^2$ electrons [85, 86].

Regarding the atomic spin densities, it is worth noting that the values of the uranium atoms are close or slightly higher than the number of unpaired electrons of the U(IV) ion, i.e. 2, whereas the values for the copper atoms are significantly lower than 1, this latter values corresponding to one unpaired electron per Cu(II) ion. These results show the localization of the two unpaired 5f electrons on the uranium ion whereas spin delocalization occurs for the unpaired

electron of the copper ions. The obtained spin density distributions (difference between the α and β electron densities) for the HS, BS1, BS2 and BS solutions obtained at the HS geometries are displayed in Figure 3. While the HS solution looks like a pure spin state solution ($<S^2> \approx 6$) the BS1, BS2 and BS solutions intrinsically do not correspond to any pure spin states. Note that the $<S^2>$ values will be later commented for the sake of extracting the coupling constants. What is important to note at this stage is that all the displayed spin densities notably involve the Cu_2O_4U cores, i.e., the path connecting the three magnetic centers. Also, in line with the description of the initial guesses (see Scheme 2, Figure 3), the spin density on the three magnetic centers is of same sign in the HS solution, one sign alternation is observed for the BS1 and BS2 solutions, and two sign alternations are observed for the BS solution.

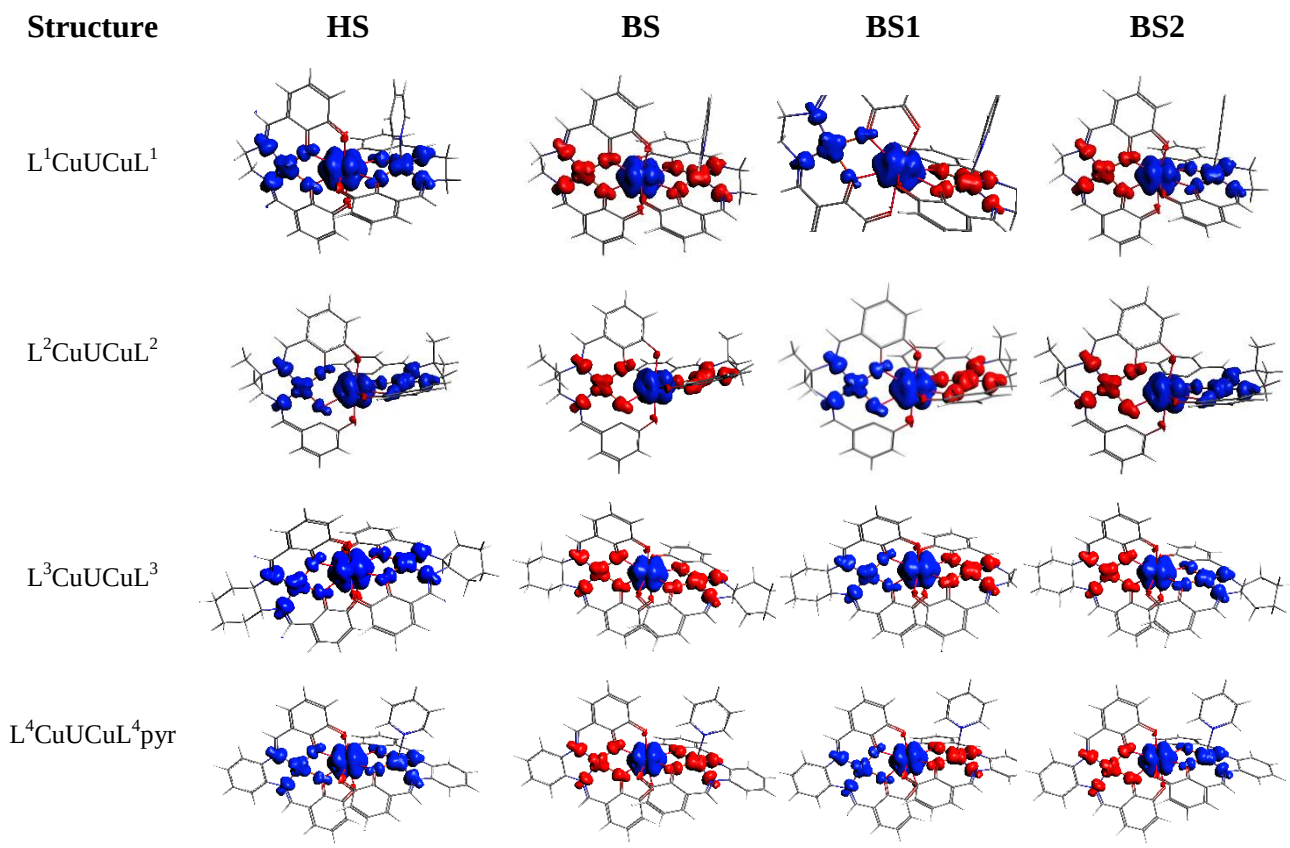

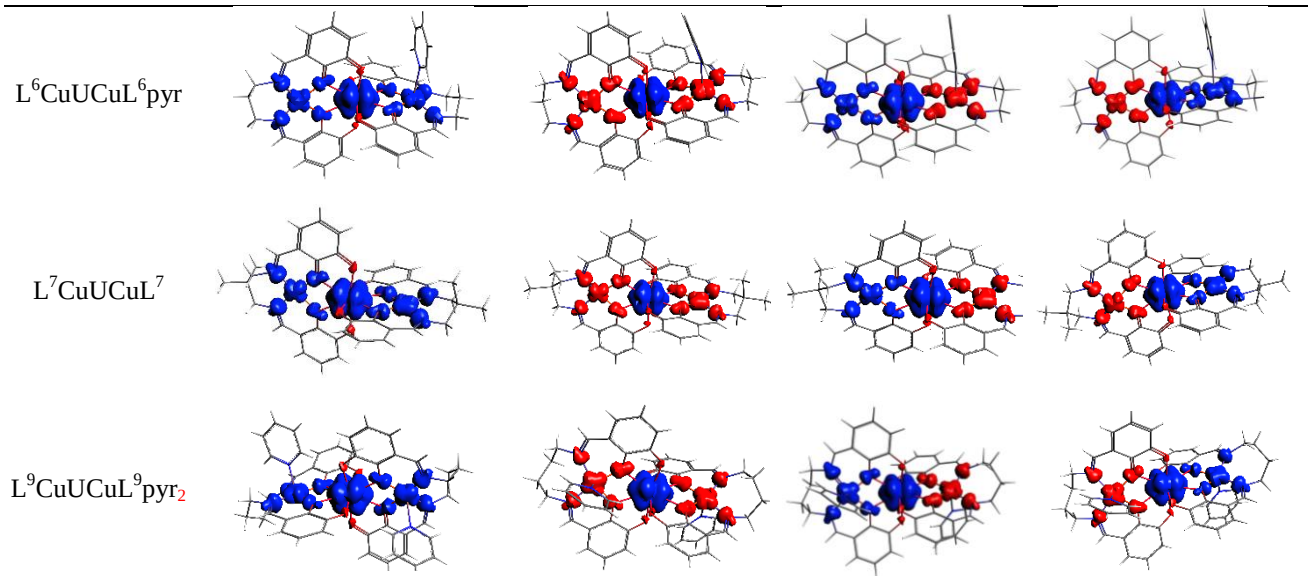

Figure 3: Representations of the ZORA/B3LYP/TZP spin densities for the HS (triplet), BS states and lower spin BS1, BS2 states of $L^{i}CuUCuL^{i}$ (I = 1-9) complexes (blue color: positive and red color: negative spin density). The isodensity surface corresponds to a value of 0.0025 e $bohr^{-3}$.

3. Magnetic properties

3.1. Evaluation of the exchange coupling constant J

We study now the magnetic exchange couplings within the considered trinuclear complexes. Experimentally, the magnetic character of these systems has been investigated by variable-temperature measurements [26, 30-34], and effective spin coupling constants derived with the subtraction method (see above).

The computation of the magnetic coupling constants is carried out using the BS approach and equations 4-10 (*vide supra*). The considered $L^{i}CuUCuL^{i}$ complexes feature the same $3d^9–5f^2–3d^9$ valence electron configurations. In Table 3, we report the total bonding energy (TBE) corresponding to the high spin (HS) and the BS spin states, as well as the lower spin BS1 and BS2 states, the unperturbed or zero energy *E*o, and the mean value of the $\langle S^2 \rangle$ operators.

From the $\langle S^2 \rangle$ values in Table 3, it is seen that the HS spin contamination is negligible ($<S^2>_{Ideal}$ = 6 for a pure quintet spin state). As already mentioned, the other three solutions do not correspond to any pure spin states. Ideally, one can expect spin contaminations that correspond to the one that would be observed at dissociation. In binuclear complexes, the ideal spin contamination can be easily obtained by using squares of Clebsch-Gordan coefficients. For

instance, for a binuclear Cu^{II}-Cu^{II} complex, the BS spin broken symmetry solution would correspond to 50% of a spin triplet and 50% of a spin singlet, resulting in an $<S^2>_{Ideal}$ value of 1. Naturally, with three magnetic centers, the determination of the $<S^2>_{Ideal}$ values is less trivial.

First, one needs to determine the full spin space by using for instance a successive coupling scheme. First, it is clear that the coupling of one $S_1 = 1/2$ site with one $S_2 = 1$ one leads to two S_{12} states: $S_{12} = 1/2$ or $S_{12} = 3/2$. Then, adding the $S_3 = 1/2$ site leads to four S_{123} states, here denoted S: one S = 2 state (the HS one), two S = 1 states, and one S = 0 state. To determine the S_{12} spin states components, one may for instance diagonalize the HDvV Hamiltonian (by construction, it generates spin functions) or simply use the appropriate Clebsch-Gordan coefficients (both approaches should eventually lead to the same exact ideal values for $<S^2>$, so the reader may freely choose his preferred scheme). In this case, the S_{12} spin states can be expressed in terms of the local M_{S1} and M_{S2} spin moments, for instance:

$$|S_{12} = \tfrac{1}{2}, M_S = \tfrac{1}{2}> = -\sqrt{\tfrac{2}{3}}\,|\mathrm{M}_{S1} = -\tfrac{1}{2}, \mathrm{M}_{S2} = 1> + \tfrac{1}{\sqrt{3}}|\mathrm{M}_{S1} = \tfrac{1}{2}, \mathrm{M}_{S2} = 0>$$

Note that the $|\mathrm{M}_{S1} = -\frac{1}{2}, \mathrm{M}_{S2} = 1>$ sub-determinant is involved in the BS2 and BS solutions (when combined with $\mathrm{M}_{S3} = \frac{1}{2}$ and $\mathrm{M}_{S3} = -\frac{1}{2}$, respectively, so that we must keep track of the $-\sqrt{\frac{2}{3}}$ coefficient. Since S_{12} = ½ in this case, the coupling coefficient with S_3 to form a pure spin singlet state is simply proportional to $\frac{1}{\sqrt{2}}$ (Clebsch-Gordan coefficient). Since we aim at squaring the coefficients (only weights are necessary), it is not mandatory to keep track of signs. Therefore, the $|\mathrm{M}_{S1} = -\frac{1}{2}, \mathrm{M}_{S2} = 1, \mathrm{M}_{S3} = -\frac{1}{2}>$ determinant bears 1/3 of pure spin singlet character. This determinant is also involved in the $|S_{12} = \frac{3}{2}, M_S = \frac{1}{2}>$ spin component, associated with a $\frac{1}{\sqrt{3}}$ coefficient:

$$|S_{12} = \tfrac{3}{2}, M_S = \tfrac{1}{2}> = \tfrac{1}{\sqrt{3}}|\mathrm{M}_{S1} = -\tfrac{1}{2}, \mathrm{M}_{S2} = 1> + \sqrt{\tfrac{2}{3}}|\mathrm{M}_{S1} = \tfrac{1}{2}, \mathrm{M}_{S2} = 0>$$

This translates into a 1/6 of spin quintet character (as before, we must also apply a coefficient proportional to $\frac{1}{\sqrt{2}}$). Consequently, this $|\mathrm{M}_{S1} = -\frac{1}{2}, \mathrm{M}_{S2} = 1, \mathrm{M}_{S3} = -\frac{1}{2}>$ determinant has 1/2 of triplet character (we do not need to distinguish the two triplet states here, if it is neither

singlet neither quintet, it can only be triplet). One can then determine the $<S^2>_{Ideal}$ value of the BS solution as:

$$\langle S^2\rangle^{BS}_{\text{Ideal}} = \frac{1}{3} * 0 + \frac{1}{2} * 2 + \frac{1}{6} * 6 = 2$$

Concerning the computation of $\langle S^2\rangle^{IS1}_{\text{Ideal}}$ or $\langle S^2\rangle^{IS2}_{\text{Ideal}}$, it is worth noting that one works within the $M_S = 1$ subspace, i.e., one can only have quintet or triplet character. Determining the quintet character (the easiest) is this enough to address the targeted value. The quintet character requires a component from the $S_{12} = 3/2$ state. In fact, expressing $|S_{12} = \frac{3}{2}, M_S = \frac{3}{2}>$ is trivial since it only arises from the $|M_{S1} = \frac{1}{2}, M_{S2} = 1>$ subdeterminant. The Clebsch-Gordan coefficient to couple this subdeterminant with an $M_{S2} = -\frac{1}{2}$ component being 1/2, the $|M_{S1} = \frac{1}{2}, M_{S2} = 1, M_{S3} = -\frac{1}{2}>$ determinant, *i.e.*, IS1, has 1/4 of quintet character, and thus, 3/4 of triplet character. Finally, we get:

$$\langle S^2\rangle^{IS1}_{\text{Ideal}} = \frac{3}{4} * 2 + \frac{1}{4} * 6 = 3 = \langle S^2\rangle^{IS2}_{\text{Ideal}}$$

Therefore, the $<S^2>$ values reported in Table 3 are practically equal to those ideal values, which is expected in the case of the weak-coupling regime.

Table 3: Computed TBE for the HS, BS, BS1 and BS2 states, zero of energy (E_0, in eV), together with the corresponding $\langle S^2\rangle$ values, for the $L^iCuUCuL^i$ X-ray (i = 2, 6, 7, 9) and model (i = 1, 3, 4) structures, with the $3d^9$–$5f^2$–$3d^9$ electron configurations.

$Cu_2UL^i pyr_x$	HS	BS	BS1	BS2	E_0	$\langle S^2\rangle$			
						HS	BS	BS1	BS2
$L^1CuUCuL^1$	–629.577518	–629.577851	–629.577769	–629.577707	–629.577711	6.01	2.01	3.01	3.01
$L^2CuUCuL^2$	–623.065403	–623.065992	–623.065664	–623.065889	–623.065737	6.01	2.00	3.01	3.01
$L^3CuUCuL^3$	–679.472075	–679.472402	–679.472758	–679.471909	–679.472286	6.01	2.00	3.01	3.01
$L^4CuUCuL^4$pyr	–709.478522	–709.478914	–709.478059	–709.479159	–709.478664	6.00	2.01	3.01	3.01
$L^6CuUCuL^6$pyr	–666.829509	–666.827766	–666.828779	–666.828591	–666.828661	6.01	1.94	3.01	3.01

$L^7CuUCuL^7$	–740.394470	–740.394041	–740.394201	–740.394345	–740.394264	6.01	2.00	2.99	3.00
$L^9CuUCuL^9pyr_2$	–783.522829	–783.522032	–783.522028	–783.522572	–783.522365	6.01	2.00	3.01	3.01

The computed exchange coupling constants J_{12} and J_{23} for adjacent Cu1---U and Cu2---U metals, and J_{13} constant for next-adjacent Cu1---Cu3 atoms are reported in Table 4.

Table 4: Computed ZORA/B3LYP/TZP exchange coupling J_{12}, J_{23}, J_{13} (cm^{-1}) constants for the $L^iCuUCuL^i$ –X-ray (i = 2, 6, 7, 9) and model (i = 1, 3, 4) structures compared to the J_{min} fitted value. Note that the J_{min} values have been multiplied by a +2 factor to match our HDvV Hamiltonian (-J convention instead of -2J).

$Cu_2UL^ipyr_x$	J_{12}	J_{23}	J_{13}	$J_{CuU} = (J_{12} + J_{23})/2$	J_{min}*
$L^1CuUCuL^1$	–1.593	–1.093	–0.860	–1.34	–3.0
$L^2CuUCuL^2$	–1.466	–3.284	–1.270	–2.38	–1.6
$L^3CuUCuL^3$	–4.734	2.105	–1.532	–1.31	–3.6
$L^4CuUCuL^4pyr$	2.855	–6.020	+1.758	–1.58	–1.0
$L^6CuUCuL^6pyr$	6.271	7.787	–0.766	7.03	+5.2
$L^7CuUCuL^7$	2.312	1.151	–0.286	1.73	+1.6
$L^9CuUCuL^9pyr_2$	5.410	1.018	+2.109	3.21	+3.8

The results show that the two exchange couplings J_{12} and J_{23} (cm^{-1}) for adjacent Cu1---U and Cu2---U metals are different due to the environmental effects around the two Cu(II) spin centers. In addition, we report in the last column the lower bound of the exchange coupling constants (J_{min}) obtained for trinuclear $L^iCuUCuL^i$ systems by experimental fitting of the magnetic susceptibility as reported by Rinehart, Long et *al*. [26]. The latter authors indicate that they could only estimate a minimum value J_{min} of the coupling constants for the complexes under consideration.

In order to compare this experimental estimation of the Cu---U coupling constant (J_{min}) [26], we have converted their values such that they are now defined with the same Hamiltonian as ours (in practice, their values have been divided by 2). Note that by neglecting J_{13} and considering equal

J_{12} and J_{23} in equation 2 (*vide supra*), J_{CuU} = (E_{BS}-E_{HS}) / 2, which also exactly matches the mean value of J_{12} and J_{23} in our previous extraction of the three coupling constants.

As it can be seen, comparing J_{CuU} and J_{min}, we reproduce correctly the AF or Ferro character of the considered complexes. The computed coupling constants fit very well the estimated ones especially for the computed complexes for which an X-ray structure is available. Moreover, the Cu1---Cu2 coupling appears weak as shown by the computed exchange J_{13} constant, which agrees well with the experimental outcomes [33-34]. Indeed, the susceptibility measurements point out the presence of a weak intramolecular AF or noninteracting Ferro coupling between these $3d^9$---$3d^9$ ions for the $L^iCuUCuL^i$ (i = 1,2,3,4) *vs*. $L^iCuUCuL^i$ (i = 6,7,9) species, respectively.

Starting from the available $L^iCuUCuL^i$ (i = 2, 6, 7, 9) X-ray structures [33-34], the modelling of the mixed $L^iCu^{II}U^{IV}Zn^{II}L^i$ systems, in which one Cu($3d^9$) paramagnetic ion is replaced by the Zn($3d^{10}$) diamagnetic center, have been considered to get more insight into the Cu^{II}---U^{IV} exchange coupling. Such diamagnetic subtraction approach has been successfully used experimentally to probe the presence of exchange coupling within actinide-containing molecules, where analogous featuring diamagnetic replacement components for the non-metal spin centers (Th^{IV}, Zn^{II}) have been synthesized, including multi-uranium, uranium-lanthanide, uranium-transition metal, and uranium-radical species [26, 33-35].

Thus, the computed HS/BS energies for the mixed $L^iCuUZnL^i$ model complexes are considered with two Zn---U/Cu1---U and Cu2---U/Zn---U sides. The one side Cu---U distance is kept fixed to its available X-ray value [33-34], while the other Zn---U side distance is optimized in their HS triplet (S =1) for each model structure. The optimized parameters, HS/BS energy states, with the corresponding $\langle S^2 \rangle$ values and exchange coupling $J_{Cu\text{-}U}$ constants are computed using the Yamaguchi formula (*vide supra*) and are reported in Table 5. Again, the reported $<S^2>$ values match the ideal ones (3.75 for a pure quartet state and 1.75 for a 1/3 quartet and 2/3 doublet mix, the weights equaling the ones previously determined for the S_{12} coupled states; those were also reported elsewhere) [70].

Table 5: Computed TBE for the HS/BS states of the mixed $L^iZnUCuL^i$ model complexes, energy difference $\Delta E = E_{BS} - E_{HS}$ (eV), $\langle S^2 \rangle_{HS/BS}$ values (exact values of are given between parentheses for comparison) and exchange magnetic coupling constant $J_{Cu\text{-}U}$ (cm^{-1}).

$ZnUCuL^i$	Zn–U/**Cu–U** (Å)	E_{HS} (eV)	E_{BS} (eV)	ΔE (eV)	$\langle S^2\rangle_{HS}$ (3.75)	$\langle S^2\rangle_{BS}$ (0.75)	$J_{Cu\text{-}U}$ (cm^{-1})
$L^1ZnUCuL^1$	3.582/**3.560**	–627.2111	–627.2124	-0.0013	3.76	1.76	–5.2
$L^2ZnUCuL^2$	3.583/**3.520**	–621.3409	–621.3414	–0.0005	3.76	1.75	–4.0
$L^3ZnUCuL^3$	3.572/**3.555**	–677.7590	–677.7593	–0.0003	3.76	1.75	–1.2
$L^4ZnUCuL^4$	3.590/**3.578**	–627.3301	–627.3309	-0.0008	3.76	1.76	–3.2
$L^6ZnUCuL^6$	3.744/**3.648**	–665.4271	–665.4251	0.0020	3.76	1.75	8.3
$L^7ZnUCuL^7$	3.748/**3.634**	–740.4001	–740.3986	0.0015	3.76	1.75	6.05
$L^9ZnUCuL^9$	3.757/**3.661**	–703.2432	–703.2425	0.0007	3.76	1.74	2.8

From Tables 5, it appears that the computed coupling constants for the mixed $L^iZnUCuL^i$ species, confirm the AF/Ferro character of the Cu^{II}---U^{IV} exchange couplings when passing from the $L^iZnUCuL^i$ (i = 1,2,3,4) to the $L^iCuUCuL^i$ (i = 6,7,9) series of complexes.

We consider now the $L^iCuThCuL^i$ complexes in which the paramagnetic $U^{IV}(5f^2)$ ion is replaced by the $Th^{IV}(5f^0)$ diamagnetic one. These complexes could allow confirming the presence or not of a magnetic exchange coupling interaction between the Cu^{II} ions. Starting from the X-ray structures $L^iCuThCuL^i$ (i = 1, 2) derivative [34], and considering the $3d^9$–$5f^0$–$3d^9$ electronic configuration, the calculations were also extended to the models (i = 3,4,6,7,9) with the HS triplet state (S = 1) $3d^\alpha$–$5f^0$–$3d^\alpha$ and BS $3d^\alpha$–$5f^0$–$3d^\beta$ one, respectively. The computation of the Cu1---Cu2 exchange coupling constant has been carried out using the Yamagushi formula [71-73]. The HS/BS energies, with the corresponding $\langle S^2\rangle$ values and exchange coupling $J_{Cu\text{--}Cu}$ constants are reported in Table 6. Once more, those values match a pure spin triplet state (2) or a 50% mixture of spin triplet and spin singlet state (1). Therefore, applying Yamagushi formula or considering as before the weak-coupling scheme is practically equivalent, as expected in this case (one should get out of the weak-coupling regime to observe significant deviations between both regimes).

Table 6: Computed TBE for the HS/BS states of the $L^iCuThCuL^i$ (i = 1-9) X-ray structures. Energy difference ΔE = $E_{BS} - E_{HS}$ (eV), $\langle S^2\rangle_{HS/BS}$ values, and magnetic exchange coupling constant $J_{Cu\text{--}Cu}$ (cm^{-1})

$L^iCuThCuL^i$	**HS**	**BS**	**ΔE(eV)**	$\langle S^2\rangle$		$J_{Cu\text{--}Cu}$ (cm^{-1})
				HS	**BS**	

$L^1CuThCuL^1$	–626.30350698	–626.30352727	–0.00002	2.00	1.00	–0.16
$L^2CuThCuL^2$	-603.52482804	-603.52488533	–0.00005	2.00	1.00	–0.40
$L^3CuThCuL^3$	-676.24159660	-676.24161297	–0.00001	2.00	1.00	–0.13
$L^4CuThCuL^4$	-706.16032211	-706.16036949	–0.00004	2.00	1.00	–0.32
$L^6CuThCuL^6$	-663.53141806	-663.53140929	0.000008	2.00	1.00	0.06
$L^7CuThCuL^7$	-736.47552598	-736.47547948	0.00004	2.00	1.00	0.37
$L^9CuThCuL^9$	–779.21030433	–779.21019057	0.00011	2.00	1.00	0.88

The results (Table 6) show that the two HS and BS states are very close in energy, leading to the very low difference (ΔE) and resulting in very weak magnetic exchange coupling between the Cu^{II} ions in good agreement with experimental outcomes, in particular for the observed weak AF Cu1---Cu2 exchange coupling of the $L^1CuThCuL^1$ and $L^2CuThCuL^2$ [2] species [33]. Indeed, it was reported that the measurement of the magnetic behaviour of such X-ray thorium $L^iCuThCuL^i$ (i = 1, 2) shows a weak intramolecular coupling between the Cu^{II} ions [34]. Moreover, the reported fitted magnetic susceptibility data, using the HDvV isotropic spin Hamiltonian $H = -JS_{Cu1}.S_{Cu2}$, with $S_{Cu1} = S_{Cu2} = ½$, led to the values of $J_{Cu\text{-}Cu} = -0.84$ and -0.48 cm^{-1} for the $L^1CuThCuL^1$ and $L^2CuThCuL^2$, respectively. In contrast, it was found [34] that for the $L^7CuThCuL^7$, the two Cu---Cu ($3d^9$---$3d^9$) ions are non-interacting or weakly ferromagnetically coupled [33]. As it can be seen in Table 6, our computations are in agreement with the experimental observations regarding the Ferro or AF character of the Cu1---Cu2 coupling.

3.2. Dependence of J_{CuU} on deformations of the Cu_2O_4U core geometry.

Small distortions of the magnetic core geometry i.e., of the Cu---U bond distances (Å) or of the bond angles Cu–O_b–U (°) (Figure 3), could lead to a significant variation of the magnetic exchange coupling constant. In the case of the trinuclear M_2Gd (M^{II} = Cu, V) complexes with the CuO_2Gd motif, it was found for the magneto-structural correlation study, that the change of the magnetic behavior from Ferro to AF was related to the increase of the bending of the core bridging angle. Furthermore, the largest AF interaction of –11.4 cm^{-1} involving gadolinium and radicals or transition metal ions was found by using a semi-quinonate radical that is a much

stronger ligand than the nitroxide-type radicals are. This result reinforced the assumption that the more tightly bound radical would favor the direct overlap of the ligand orbitals with the 5f orbitals, leading to antiferromagnetism, over the overlap with the s and d orbitals that leads to ferromagnetism [86]. The former interaction could become dominant in the uranium complexes because of the greater spatial extension of the 5f orbitals. Thus, bringing the Cu^{II} and U^{IV} ions closer in the Cu_2UL^i complexes resulting in a decrease of the Cu–O_b–U angle, could cause the change from Ferro to AF. Therefore, to get a deeper insight into the crucial role of the Cu_2O_4U core geometry on the magnetic exchange, the coupling constant $J_{Cu\text{-}U}$ was computed for the L^1CuUCuL^1pyr AF model complex considering different Cu---U bond distances (Å), corresponding to different Cu–O_b–U (°) bond angles. The geometry of the L^1CuUCuL^1pyr complex model is optimized keeping the Cu_2O_4U core geometry fixed at each Cu---U bond distances from 3.50 to 3.65 Å**.**

Precisely, the computation of the $J_{Cu—U}$ constants is carried out for different fixed cores structures fc1-5 with Cu---U distances varying symmetrically from 3.50 to 3.65 Å for the L^1CuUCuL^1pyr model complex. By the way, the relative stability of the different optimized L^1CuUCuL^1pyr model geometries towards the Cu_2O_4U distortions could be checked. The most stable structure is obtained for a Cu---U distance equal to 3.55 Å whereas distances higher than 3.65 Å lead to structures exhibiting energies higher than 3 kcal/mol relatively to the most stable geometry.

In Table 7, are reported the ZORA/B3LYP/TZP computed energies (eV) of the HS, BS states and the $J_{Cu\text{-}U}$ constant for the fc1-5 structures. In this Table, the <Cu–O–U> value is the average of the Cu1-O-U and Cu2-O-U angles.

Table 7: Computed HS and BS TBE (eV) and exchange coupling $J_{Cu\text{-}U}$ of the different fc1-5 structures of the model complex L^1CuUCuL^1pyr.

fixed core	Cu---U (Å)	<Cu–O–U> (°)	HS	BS	$J_{Cu\text{-}U}$
fc1	3.50	108.9	–628.634434	–628.634803	–2.98
fc2	3.55	109.8	–628.665128	–628.665485	–2.88
fc3	3.60	110.8	–628.564672	–628.564997	–2.62

fc4	3.62	111.2	–628.476657	–628.476932	–2.22
fc5	3.65	111.7	–628.313549	–628.313768	–1.77

Notably, the results in Table 7 indicate that the magnitude of the J_{CuU} constants of such species are closely related to the geometry of the bridging Cu_2O_4U core, its value diminishing significantly with the lengthening of the Cu---U distance. Such decrease of the coupling constants suggests a shift from AF to Ferro character for higher Cu---U distances and Cu-O-U angles.

The frontier MO diagram of the $L^1CuUCuL^1pyr$ fc1-5 models in the HS (S = 2) state, is shown on Figure 4. This diagram is composed of three distinct blocs of MO levels; the highest levels are the two degenerate α singly occupied SOMO and SOMO-1 with energy splitting of *ca*. 0.14 eV, and immediately below, are located the Schiff base molecular levels followed by the Cu_2O_4U core MOs. Furthermore, the SOMO and SOMO-1 (Figure 5) seem to be destabilized and the LUMO is stabilized with the Cu—O_b—U angle opening, the SOMO – LUMO splitting decreasing from 1.734 to 1.404 eV. Notably, the SOMO-24 and SOMO-25 displaying the two $Cu(d^9)$---$Cu(d^9)$ MO character as shown by their isodensity surface (Figure 5), are magnetically perturbed, highly delocalized and deeper in energy relatively to the SOMO/SOMO-1.

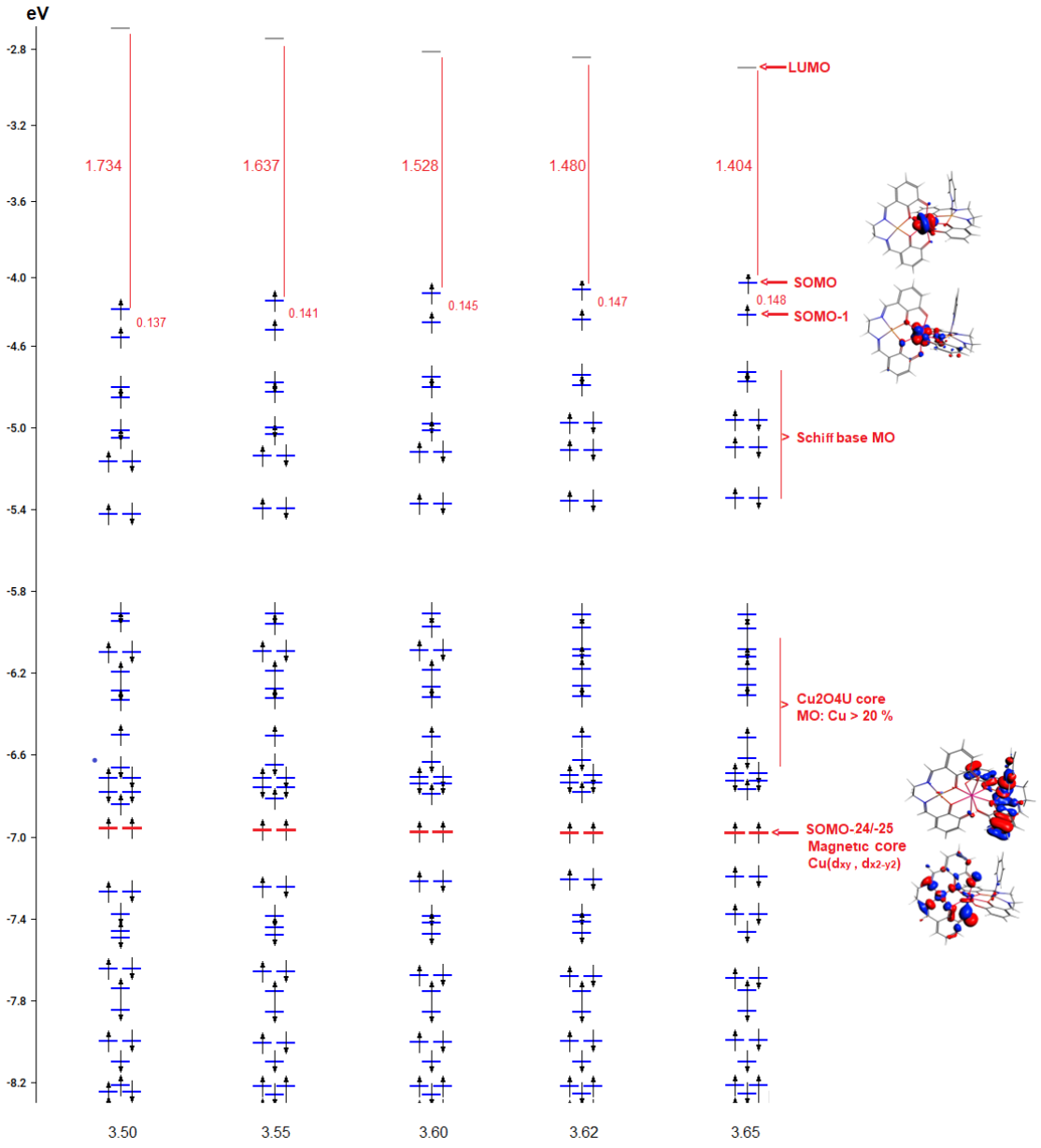

Figure 4: ZORA/B3LYP/TZP MO diagrams of the HS state of the $L^1CuUCuL^1pyr$ models for different Cu--U bond distances from 3.50 to 3.65 Å.

In Table 8, are reported the ZORA/B3LYP/TZP computed energies and orbital contributions to the SOMO and SOMO-1 as well as to the SOMO-24/-25 for the $L^1CuUCuL^1pyr$ model complexes for different Cu---U distances. Is also reported for comparison, the MO composition of the Ferro $L^6CuUCuL^6pyr$ species for a Cu—U distance equal to 3.65 Å. The $Cu–O_b/O_b–U$ Mayer and Nalewajski-Mrozek (NM) bond orders also reported with the Cu---U

(Å) distance variation. The <Cu–O_b–U> (°) angle corresponds to the average variation of the two Cu1–O_b–U and Cu2–O_b–U angles.

Table 8: ZORA/B3LYP/TZP computed most relevant orbital contributions to the SOMOs of the AF L^1CuUCuL^{1}pyr model complex for different Cu--U (Å) distances and corresponding Cu–O_b/O_b–U Mayer and NM average bond orders. Last row, results for the ferromagnetic L^6CuUCuL^{6}pyr complex at a Cu--U distance equal to 3.65Å.

fixed core	Cu--U (Å)	*Energy (eV)* % (U(6d/5f) / CuL / Cu(3d) / O(2p)) SOMO	SOMO–1	SOMO-24	SOMO-25	<Cu1/2—O> <O—U> Mayer	NM
				L^1CuUCuL^{1}pyr			
fc1	3.50	–4.422 86.5/0/0/0	–4.559 79/4.6/0/7.6	–7.001 5.0/54.3/6.3/37.2	–7.059 4.4/65.0/2.3/62.5	0.401 0.187	0.833 1.171
fc2	3.55	–4.380 90.7/0/0/0	–4.521 74.0/0/0/6.3	–6.961 4.9/55.3/5.6/43.1	–7.021 2.1/63.2/3.0/60.2	0.402 0.191	0.823 1.169
fc3	3.60	–4.340 91.6/0/0/0	–4.485 91.4/0/0/6.1	–6.968 0/59.7/3.8/50.0	–7.022 0/60.4/6.7/53.6	0.408 0.180	0.813 1.167
fc4	3.62	–4.324 90.7/0/0/0	–4.471 89.4/0/0/6.0	–6.961 0/60.8/3.2/51.9	–7.017 0/58.7/7.6/51.0	0.410 0.182	0.809 1.166
fc5	3.65	–4.201 91.5/0/0/0	–4.449 91.2/0/0/5.9	–6.960 0/61.1/2.2/57.6	–7.042 0/55.6/10.8/36.0	0.413 0.186	0.803 1.165
				L^6CuUCuL^{6}pyr			
	3.65	–3.990 93.9/0/0/0	–4.199 90.6/0/0/0	–6.726 0/61.9/8.1/59.3	-6.859 0/64.3/10.8/59.6	0.418 0.181	0.847 1.162

Notably, the results of the L^1CuUCuL^{1}pyr complex models (Table 8) confirm that the SOMO and SOMO-1 are mainly 5f orbitals (weight > 90 %) with no contribution from the Cu orbitals, while the SOMO-24 and SOMO-25, deeper in energy, are Schiff base MOs with significant Cu(3d) orbitals (2.2 < Cu < 10.8 %).

The SOMO-25 spin-orbital is representative of the orbital mixing of the atoms of the magnetic core. The results of the Table 8 show that the percentage of the oxygen (2p) orbitals contribution to the SOMO-25 decreases slightly when the Cu---U distance is increased. In the same way, the weight of the uranium orbitals decreases drastically and is equal to zero when this distance is

equal or higher to 3.60 Å. This overall decrease of the weights of the oxo-bridging (2p) and uranium orbitals in SOMO-25 with the lengthening of the Cu---U distance, disfavors the Cu—U superexchange interactions thus likely explaining the decrease of the AF coupling constant.

As observed for the L^1CuUCuL^{1}pyr model complexes, the ferromagnetic L^6CuUCuL^{6}pyr species (Table 8) for the same Cu---U distance (3.65 Å), exhibits no contribution of the uranium orbitals for the two SOMO-24 and SOMO/-25, so disfavoring the superexchange interactions that could lead to the AF character. Moreover, considering the variation of the J_{Cu-U} coupling constant for the L^6CuUCuL^{6}pyr complex when reducing the Cu---U distance (Table S1) it appears that its ferromagnetic character diminishes accordingly. Even more, an AF character could be reached for Cu—U distances lower or equal to 3.59 Å. Looking at the MOs of L^6CuUCuL^{6}pyr describing the magnetic core it is seen, similarly to the L^1CuUCuL^{1}pyr case, that the weight of uranium orbitals in these MOs is no longer null and increases for distances shorter to 3.61 Å, thus triggering the superexchange responsible of the AF character.

.

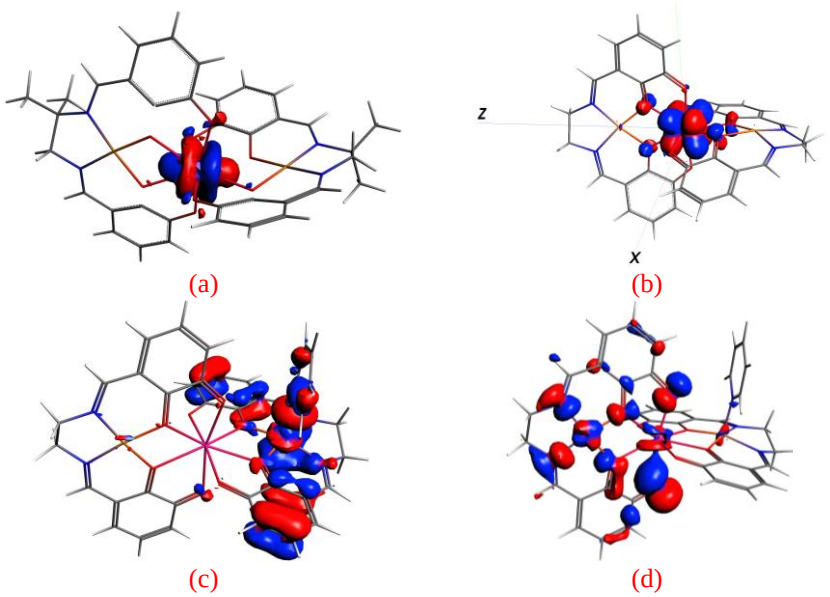

Figure 5: Iso-surfaces density maps of the (a) SOMO, (b) SOMO-1, (c) SOMO-24 and (d) SOMO-25 or the L^1CuUCuL^{1}pyr complex (isodensity surface at 0.0025 e bohr^{-3})

Regarding the variation of the Mayer and NM bond orders in the fc1-5 series (Table 8) it can be seen that their values remain high, in line with the covalent character of the bindings.

Conclusion:

In summary, the exchange coupling constants between Cu(II) and U(IV) paramagnetic centers in a series of trinuclear Schiff base bridged $L^iMAnML^i(pyr)_x$ (M^{II} = Zn, Cu; An^{IV} = Th, U; L = Schiff base; i = 1-4, 6, 7, 9; x = 0-2) complexes, have been investigated theoretically using relativistic DFT computations at the ZORA/B3LYP/TZP level, combined with the broken symmetry (BS) approach. The considered uranium complexes exhibit a double oxo-bridged $[Cu(\mu\text{-}O)]_2U$ core, with Cu---U adjacent centers and Cu---Cu next-adjacent ones. The uranium environment is the same in all complexes. The shift from antiferromagnetic (AF) character to ferromagnetic (Ferro) observed experimentally for the Cu---U coupling, when passing from the $L^iCuUCuL^i$ (i = 1,2,3,4) series to the $L^iCuUCuL^i$ (I = 6,7,9) series for different diimino backbones is confirmed by the calculations. The computations indicate a moderate magnetic exchange coupling constant J_{CuU}, with lower and upper bounds $-2.38 < J < +7.03$ cm^{-1}, in good agreement with the available experimental fitted values ($-3.6 < J_{min} < +5.2$ cm^{-1}). This AF/Ferro shift is confirmed by the study of the mixed $L^iZnUCuL^i$ species whereas consideration of the $L^iCuThCuL^i$ series of complexes permitted to confirm the expected small value of the Cu---Cu coupling constant. The influence of small changes of the Cu---U distance and Cu–O–U angle on the coupling constants has been investigated considering the $L^iCuUCuL^i$ model. Although the robust magnetic exchange coupling within the Cu_2O_4U cores is generally maintained when small variations of the core geometry are applied, it is shown in the case of the $L^1CuUCuL^1pyr$ model that the AF character diminishes with the opening of the Cu–O–U angle. For large Cu---U distances it has been shown that the weight of the uranium orbitals in the magnetic core decreases drastically limiting the superexchange responsible of the AF character. The same phenomenon for the same reason appears considering the ferromagnetic $L^6CuUCuL^6pyr$ complex; the J_{CuU} coupling constant diminishes when reducing the Cu---U distance, leading to an AF character for small distances. The combined structural and electronic analysis data were corroborated by the MO analysis sustaining that the Cu---U electronic communication favouring

magnetic superexchange interactions in such trinuclear $L^{i}CuUCuL^{i}$ systems, originates partially from the covalently bound Cu–O–U oxo-bridges in the Cu_2O_4U core.

Supplementary Information

-Optimized coordinates

Supplementary data to this article can be found online.

Acknowledgments

The authors are grateful to Frères Mentouri University of Constantine 1 and the Centre de Recherche en Sciences Pharmaceutiques CRSP (Algeria) for providing computing facilities. Are also acknowledged, the Algerian PRFU project (2022-2024: Grant No. B00L01EN250120220001) and the French GENCI IDRIS and GENCI-CINES for an allocation of computing time (Grant No. 2021-080649).

References:

1. Bencini, A.; Benelli, C.; Caneschi, A.; Carlin, R. L.; Dei, A.; Gatteschi, D. Crystal and molecular structure of and magnetic coupling in two complexes containing gadolinium(III) and copper(II) ions. J. Am. Chem. Soc. **1985**, 107, 8128-8136. https://doi.org/10.1021/ja00312a054
2. Bencini, A.; Benelli, C.; Caneschi, A.; Dei, A.; Gatteschi, D. Crystal and molecular structure and magnetic properties of a trinuclear complex containing exchange-coupled Cu_2Gd species. Inorg. Chem. **1986**, 25, 572-575. https://doi.org/10.1021/ic00224a036
3. Ahmed, N.; Sharma, T.; Spillecke, L.; Koo, C.; Ansari, K., U.; Tripathi, S.; Caneschi, A.; Klingeler, R.; Rajaraman, G.; Shanmugam, M.. Probing the Origin of Ferro-/Antiferromagnetic Exchange Interactions in Cu(II)–4f Complexes. Inorg. Chem. **2022**, 61, 5572-5587. https://doi.org/10.1021/acs.inorgchem.2c00065
4. Rajaraman, G.; Totti, F.; Bencini, A.; Caneschi, A.; Sessoli, R.; Gatteschi, D. Density functional studies on the exchange interaction of a dinuclear Cu(II)–Gd(III) complex:

method assessment, magnetic coupling mechanism and magneto-structural correlations. Dalton Trans., **2009**, 3153–3161. https://doi.org/10.1039/b817540c

5. Liu, K.; Shi, W.; Cheng, P. Toward heterometallic single-molecule magnets: Synthetic strategy, structures and properties of 3d–4f discrete complexes. Coord. Chem. Rev., **2015**, 289–290, 74–122; https://doi.org/10.1016/j.ccr.2014.10.004

6. Maity, S.; Mondal, A.; Konar, S.; Ghosh, A. The role of 3d–4f exchange interaction in SMM behaviour and magnetic refrigeration of carbonato bridged $Cu^{II}_2Ln^{III}_2$ (Ln = Dy, Tb and Gd) complexes of an unsymmetrical N_2O_4 donor ligand. Dalton Trans., **2019**, 48, 15170. https://doi.org/10.1039/C9DT02627D

7. Dey, A.; Bag, P.; Kalita, P.; Chandrasekhar, P. Heterometallic Cu^{II}–Ln^{III} complexes: Single molecule magnets and magnetic refrigerants. Coord. Chem. Rev., **2021**, 432, 213707. https://doi.org/10.1016/j.ccr.2020.213707

8. Benelli, C.; Gatteschi, D. Magnetism of Lanthanides in Molecular Materials with Transition-Metal Ions and Organic Radicals. Chem. Rev. **2002**, 102, 2369-2387. https://doi.org/10.1021/cr010303r

9. Peng, J.-B.; Zhang, Q.-C.; Kong, X.-J.; Zheng, Y.-Z.; Ren, Y.-P.; Long, L.-S.; Huang, R.-B.; Zheng, L.-S.; Zheng, Z. High-Nuclearity 3d–4f Clusters as Enhanced Magnetic Coolers and Molecular Magnets. J. Am. Chem. Soc., **2012**, 134, 3314–3317. https://doi.org/10.1021/ja209752z

10. Song, X.-Q.; Xia, X.-L.; Song, F.-Q.; Liu, G.-H.; Wang, L. Tuning the coordination behavior of an unexplored asymmetric multidentate ligand for developing diverse heterometallic architectures with luminescent and magnetic properties. Cryst. Eng. Comm., **2021**, 23, 1000. https://doi.org/10.1039/D0CE01298J

11. Jesudas, J. J.; Pham, C. T.; Hagenbach, A.; Abram, U.; Nguyen, H. H. Trinuclear $Co_2^{II}Ln^{III}$ Complexes (Ln = La, Ce, Nd, Sm, Gd, Dy, Er, and Yb) with 2,6-Dipicolinoylbis(N,N-diethylthiourea): Synthesis, Structures, and Magnetism. Inorg. Chem. **2020**, 59, 386-395. https://doi.org/10.1021/acs.inorgchem.9b02648

12. Ruiz, E.; Cano, J.; Alvarez, S.; Alemany, P. Broken Symmetry Approach to Calculation of Exchange Coupling Constants for Homobinuclear and Heterobinuclear Transition Metal Complexes. J. Comput. Chem. 1999, 20, 1391-1400. https://doi.org/10.1002/(SICI)1096-987X(199910)20:13<1391::AID-JCC6>3.0.CO;2-J

13. Yan, F.; Chen, Z. Magnetic Coupling Constants and Spin Density Maps for Heterobinuclear Complexes $GdCu(OTf)_3(bdmap)_2(H_2O)THF$, $[Gd(C_4H_7ON)_4(H_2O)_3][Fe(CN)_6]_2H_2O$, and $[Gd(C_4H_7ON)_4(H_2O)_3][Cr(CN)_6]_2H_2O$: A Density Functional Study. J. Phys. Chem. A, **2000**, 104, 6295-6300. https://doi.org/10.1021/jp994093m

14. Rudra, I.; Raghu, C.; Ramasesha, S. Exchange interaction in binuclear complexes with rare-earth and copper ions: A many-body model study. Phys. Rev. B **2002**, 65, 224411. https://doi.org/10.1103/PhysRevB.65.224411

15. Ruiz, E. (**2004**). Theoretical Study of the Exchange Coupling in Large Polynuclear Transition Metal Complexes Using DFT Methods. In: Principles and Applications of Density Functional Theory in Inorganic Chemistry II. Structure and Bonding, vol 113. Springer, Berlin, Heidelberg. https://doi.org/10.1007/b97942

16. Neese, F. Prediction of molecular properties and molecular spectroscopy with density functional theory: From fundamental theory to exchange-coupling. Coord. Chem. Rev. **2009**, 253, 526-563. https://doi.org/10.1016/j.ccr.2008.05.014

17. Døssing, A. Recent advances in the coordination chemistry of hydroxo-bridged complexes of chromium(III) Author links open overlay panel. Coord. Chem. Rev. **2014**, 280, 38-53. https://doi.org/10.1016/j.ccr.2014.08.005

18. David, G.; Wennmohs, F.; Neese, F.; Ferré, N. Chemical Tuning of Magnetic Exchange Couplings Using Broken-Symmetry Density Functional Theory. Inorg. Chem. **2018**, 57, 12769-12776. https://doi.org/10.1021/acs.inorgchem.8b01970

19. Sheng, X.; Thompson, L.,M.; Hratchian, H. P. Assessing the Calculation of Exchange Coupling Constants and Spin Crossover Gaps Using the Approximate Projection Model To Improve Density Functional Calculations. J. Chem. Theory Comput. **2020**, 16, 154−163. https://doi.org/10.1021/acs.jctc.9b00387

20. Cirera, J.; Jiang, Y.; Qin, L.; Zheng, Y.-Z.; Li, G.; Wu, G.; Ruiz, E. Ferromagnetism in polynuclear systems based on non-linear [$Mn^{II}_2Mn^{III}$] building blocks. Inorg. Chem. Front. **2016**, 3, 1272–1279. https://doi.org/10.1039/C6QI00189K

21. Speed, S., Pointillart, F., Mulatier, J.-C., Guy, L., Golhen, S., Cador, O., Le Guennic, B., Riobé, F., Maury, O., Ouahab, L. Photophysical and Magnetic Properties in Complexes Containing 3d/4f Elements and Chiral Phenanthroline-Based Helicate-Like Ligands. Eur. J. Inorg. Chem. **2017**, 2100–2111. https://doi.org/10.1002/ejic.201601501

22. Cremades, E.; Gómez-Coca, S.; Aravena, D.; Alvarez, S.; Ruiz, E. Theoretical Study of Exchange Coupling in 3d-Gd Complexes: Large Magnetocaloric Effect Systems. J. Am. Chem. Soc. **2012**, 134, 10532–10542. https://doi.org/10.1021/ja302851n

23. Kahn, M. L.; Mathoniere, C.; Kahn, O. Nature of the Interaction between Ln^{III} and Cu^{II} Ions in the Ladder-Type Compounds $\{Ln_2[Cu(opba)]_3\}\cdot S$ (Ln = Lanthanide Element; opba = ortho-Phenylenebis(oxamato), S = Solvent Molecules). Inorg. Chem. **1999**, 38, 3692. https://doi.org/10.1021/ic9811998

24. Paulovic, J.; Cimpoesu, F.; Ferbinteanu, M.; Hirao, K. Mechanism of Ferromagnetic Coupling in Copper(II)-Gadolinium(III) Complexes J. Am. Chem. Soc. **2004**, 126, 3321-3331. https://doi.org/10.1021/ja030628k

25. Benelli, C.; Gatteschi, D. Magnetism of Lanthanides in Molecular Materials with Transition-Metal Ions and Organic Radicals. Chem. Rev. **2002**, 102, 2369. https://doi.org/10.1021/cr010303r

26. Rinehart, J. D.; Harris, T.D.; Kozimor, S.A.; Bartlett, B.M. Long, J.R. Magnetic Exchange Coupling in Actinide-Containing Molecules, Inorg. Chem., **2009**, 48, 3382-3395. https://doi.org/10.1021/ic801303w

27. Lukens, W.W.; Speldrich, M.; Yang, P.; Duignan, T.J.; Autschbach, J.; Kögerler, P. The roles of 4f- and 5f-orbitals in bonding: A magnetochemical, crystal field, density functional theory, and multi-reference wavefunction study. Dalton Trans. 2016, 45, 11508–11521. https://doi.org/10.1039/c6dt00634e

28. Ephritikhine, M. The vitality of uranium molecular chemistry at the dawn of the XXIst century. Dalton Trans. **2006**, 2501. https://doi.org/10.1039/b603463b

29. Belkhiri, L.; Le Guennic, B.; Boucekkine, A. DFT Investigations of the Magnetic Properties of Actinide Complexes. Magnetochemistry 2019, 5, 15. https://doi.org/10.3390/magnetochemistry5010015

30. Le Borgne, T.; Rivière, E.; Marrot, J.; Girerd, J.-J.; Ephritikhine, M. Synthesis, Crystal Structure, and Magnetic Behavior of Linear $M_2^{II}U^{IV}$ Complexes (M= Co, Ni, Cu, Zn). Angew. Chem. Ed. Int. **2000**, 39, 1647-1649. https://doi.org/10.1002/(SICI)1521-3757(20000502)112:9<1713::AID-ANGE1713>3.0.CO;2-V

31. Salmon, L.; Thuéry, P.; Rivière, E.; Marrot, J.; Girerd, J.-J.; Ephritikhine, M. Syntheses, X-Ray Crystal Structures, and Magnetic Properties of Novel Linear $M^{II}{}_2U^{IV}$ Complexes (M = Co, Ni, Cu, Zn). Chem. Eur. J. **2002**, 8,773–783. https://doi.org/10.1002/1521-3765(20020215)8:4<773::AID-CHEM773>3.0.CO;2-1

32. Salmon, L.; Thuéry, P.; Ephritikhine, M. Crystal structure of hetero(bi- and tetra-)metallic complexes of compartmental Schiff bases uniting uranyl and transition metal (Ni^{2+}, Cu^{2+}) ions. Polyhedron, **2003**, 22, 2683-2688. https://doi.org/10.1016/S0277-5387(03)00366-8

33. Salmon, L.; Thuéry, P.; Rivière, E.; Girerd, J.-J.; Ephritikhine, M. Versatility of the nature of the magnetic Cu(II)–U(IV) interaction. Syntheses, crystal structures and magnetic properties of Cu_2U and CuU compounds. Dalton Trans. **2003**, 2872–2880. https://doi.org/10.1039/B304414A

34. Salmon, L.; Thuéry, P.; Rivière, E.; Girerd, J.-J.; Ephritikhine, M. Synthesis, Structure, and Magnetic Behavior of a Series of Trinuclear Schiff Base Complexes of 5f (U^{IV},Th^{IV}) and 3d (Cu^{II}, Zn^{II}) Ions. Inorg. Chem. **2006**, 45, 83–93. https://doi.org/10.1021/ic0512375

35. Lukens, W.W.; Walter, M.D. Quantifying Exchange Coupling in f-Ion Pairs Using the Diamagnetic Substitution Method. Inorg. Chem. **2010**, 49, 4458–4465. https://doi.org/10.1021/ic100120d

36. Kozimor, S.A.; Bartlett, B.M.; Rinehart, J.D.; Long, J.R. Magnetic Exchange Coupling in Chloride-Bridged 5f-3d Heterometallic Complexes Generated via Insertion into a Uranium(IV) Dimethylpyrazolate Dimer. J. Am. Chem. Soc. **2007**, 129, 10672–10674. https://doi.org/10.1021/ja0725044

37. Rinehart, J. D. Bartlett, B. M. Kozimor, S. A. Long, J. R. Ferromagnetic exchange coupling in the linear, chloride-bridged cluster (cyclam)CoII[(l-Cl)UIV(Me2Pz)4]2. Inorg. Chim. Acta **2008**, 361, 3534–3538. https://doi.org/10.1016/j.ica.2008.03.006

38. Monreal, M.J.; Carver, C.T.; Diaconescu, P.L. Redox Processes in a Uranium Bis(1,10-diamidoferrocene) Complex. Inorg. Chem. **2007**, 46, 7226–7228. https://doi.org/10.1021/ic700457h

39. Teyar, B.; Belkhiri, L.; Costuas, K.; Boucekkine, A.; Meyer, K. Electronic Structure and Magnetic Properties of Dioxo-Bridged Diuranium Complexes with Diamond-Core Structural Motifs: A Relativistic DFT Study. Inorg. Chem. **2016**, 55, 2870–2881. https://doi.org/10.1021/acs.inorgchem.5b02704

40. Teyar, B.; Boucenina, S.; Belkhiri, L.; Le Guennic, B.; Boucekkine, A.; Mazzanti. M. Theoretical investigation of the electronic structure and magnetic properties of oxo-bridged uranyl based dinuclear and trinuclear complexes. Inorg. Chem. **2019**, 58, 10097-10110. https://doi.org/10.1021/acs.inorgchem.9b01237

41. te Velde, G.; Bickelhaupt, F. M.; Baerends, E. J.; Fonseca Guerra, C.; van Gisbergen, S. JJ; A., Snijder, J. G.; Ziegler, T. Chemistry with ADF. J. Comput. Chem. **2001**, 22, 931-967. https://doi.org/10.1002/jcc.1056

42. AMS 2021.107, SCM, Theoretical Chemistry, Vrije Universiteit, Amsterdam, The Netherlands, R. Rüger, M. Franchini, T. Trnka, A. Yakovlev, E. van Lenthe, P. Philipsen, T. van Vuren, B. Klumpers, T. Soini. http://www.scm.com

43. van Lenthe, E.; Baerends, E. J.; Snijders, J. G. Relativistic regular two-component Hamiltonians. J. Chem. Phys. **1993**, 99, 4597-4610. https://doi.org/10.1063/1.466059

44. van Lenthe, E., Ehlers, A. E.; Baerends E. J. Geometry optimization in the Zero Order Regular Approximation for relativistic effects, J. Chem. Phys. 1999, 110, 8943-8953. https://doi.org/10.1063/1.478813

45. Becke, A. D. Density-functional exchange-energy approximation with correct asymptotic behaviour. Phys. Rev. A, **1988**, 38: 3098−3100. https://doi.org/10.1103/PhysRevA.38.3098.

46. Perdew, J. P. Density-functional approximation for the correlation energy of the inhomogeneous electron gas. Phys. Rev. B, **1986**, 33, 8822−8824. https://doi.org/10.1103/PhysRevB.33.8822

47. Boucenina, S.; Belkhiri, L.; Meskaldji, S.; Linguerri, R.; Chambaud, G.; Boucekkine, A.; Hochlaf. M. Electronic structure and magnetic properties of naphthalene- and stilbene-

diimide-bridged diuranium(V) complexes: A theoretical study. J. Mol. Model. **2020**, 26, 282 https://doi.org/10.1007/s00894-020-04552-9

48. Reta, D.; Ortu, F.; Randall S.; Mills, D. P.; Chilton, N. F.; Winpenny, R. E. P;. Natrajan, L.; Edwards, B.; Kaltsoyannis, N. (2018) The performance of density functional theory for the description of ground and excited state properties of inorganic and organometallic uranium compounds. J. Organomet. Chem. **2018**, 857, 58–74. https://doi.org/10.1016/j.jorganchem.2017.09.021

49. Meskaldji, S.; Belkhiri, A.; Belkhiri, L.; Boucekkine, A.; Ephritikhine, M. Magnetic exchange coupling in imido bimetallic uranium(V) complexes. A relativistic DFT study. C R. Chimie **2012**, 15, 184-191. https://doi.org/10.1016/j.crci.2011.07.006

50. Meskaldji, S.; Zaiter, A.; Belkhiri, L.; Boucekkine, A. A relativistic DFT study of magnetic exchange coupling in ketimide bimetallic uranium(IV) complexes. Theor. Chem. Acc. **2012**, 131, 1151. https://doi.org/10.1007/s00214-012-1151-9

51. Gaunt, A. J.; Reilly, S. D.; Enriquez, A. E.; Scott, B. L.; Ibers, J. A.; Sekar, P.; Ingram, K. I. M.; Kaltsoyannis, N.; Neu, M. P. Experimental and Theoretical Comparison of Actinide and Lanthanide Bonding in $M[N(EPR_2)2]_3$ Complexes (M = U, Pu, La, Ce; E = S, Se, Te; R = Ph, iPr, H). Inorg. Chem. **2008**, 47, 29−41. https://doi.org/10.1021/ic701618a

52. Graves, C. R.; Yang, P.; Kozimor, S. A.;Vaughn, A. E.; Clark, D. L.; Conradson, S. D.; Schelter, E. J.; Scott, B. L.; Thompson, J. D.; Hay P. J.; Morris, D. E.; Kiplinger, J. L. Organometallic Uranium(V)−Imido Halide Complexes: From Synthesis to Electronic Structure and Bonding. J. Am. Chem. Soc. **2008**, 130, 5272–5285 https://doi.org/10.1021/ja711010h

53. Rajaraman, G.; Totti, F.; Bencini, A.; Caneschi, A.; Sessoli, R.; Gatteschi, D. Density functional studies on the exchange interaction of a dinuclear Gd(III)–Cu(II) complex: method assessment, magnetic coupling mechanism and magneto-structural correlations. Dalton. Trans. **2009**, 3153−3161. https://doi.org/10.1039/B817540C

54. Spencer, L. P.; Schelter, E. J.; Yang, P.; Gdula, R. L.; Scott, B. L.; Thompson, J. D.; Kiplinger, J. L.; Batista, E. R.; Boncella, J. M. Cation-cation interactions, magnetic communication, and reactivity of the pentavalent uranium ion $[U(NtBu)_2]^+$. Angew. Chem. Int. Ed. **2009**, 48, 3795–3798. https://doi.org/10.1002/anie.200806190

55. Newell, B. S.; Rapp, A. K.; Shores, M. P. Experimental Evidence for Magnetic Exchange in Di- and Trinuclear Uranium(IV) Ethynylbenzene Complexes. Inorg. Chem. **2010**, 49: 1595–1606. https://doi.org/10.1021/ic901986w

56. Peralta, J. E.; Melo, J. I. Magnetic Exchange Couplings with Range-Separated Hybrid Density Functionals. J. Chem. Theory Comput. **2010**, 6, 1894−1899. https://doi.org/10.1021/ct100104v

57. Páez-Hernández, D.; Murillo-López, J. A.; Arratia-Pérez, R. Optical and Magnetic Properties of the Complex Bis(dicyclooctatetraenyl)diuranium. A Theoretical View. Organometallics **2012,** 31, 6297−6304. https://doi.org/10.1021/om300560h

58. Becke, A. D. Density-functional thermochemistry. III. The role of exact exchange. J. Chem. Phys. **1993**, 98, 5648. https://doi.org/10.1063/1.464913

59. Lee, C.; Yang, W.; Parr, R. G. Development of the Colle-Salvetti correlation-energy formula into a functional of the electron density. Phys. Rev. B **1988**, 37, 785. https://doi.org/10.1103/PhysRevB.37.785

60. Noodleman, L.J.; Davidson, E. R. Ligand spin polarization and antiferromagnetic coupling in transition metal dimers. J. Chem. Phys. **1986**, 109, 131–143. https://doi.org/10.1016/0301-0104(86)80192-6

61. Noodleman, L. J.; Peng, C. Y.; Case, D. A.; Mouesca, J. M. Orbital interactions, electron localization and spin coupling in iron-sulfur clusters. Coord. Chem. Rev. **1995**, 144, 199–244. https://doi.org/10.1016/0010-8545(95)07011-L

62. Døssing, A. Recent advances in the coordination chemistry of hydroxo-bridged complexes. Coord. Chem. Rev. **2014**, 280, 38–53. https://doi.org/10.1016/j.ccr.2014.08.005

63. Neese, F. Prediction of molecular properties and molecular spectroscopy with density functional theory: From fundamental theory to exchange coupling. Coord. Chem. Rev. **2009**, 253, 526−563. https://doi.org/10.1016/j.ccr.2008.05.014

64. Selmi, W.; Abdelhak, J.; Marchivie, M.; Chastanet, G.; Zid, M. F. An investigation by DFT of the electronic structure and magnetic properties of a novel l-oxo-iron(III) complex with the 1,10-phenathroline ligand. Polyhedron **2017**, 123, 441–452. https://doi.org/10.1016/j.poly.2016.12.012

65. Moreira, I.D.; Costa, R.; Filatov, M.; Illas, F. Restricted Ensemble-Referenced Kohn–Sham versus Broken Symmetry Approaches in Density Functional Theory: Magnetic Coupling in Cu Binuclear Complexes. J. Chem. Theory Comput. **2007**, 3, 764–774. https://doi.org/10.1021/ct7000057

66. Onofrio, N.; Mouesca, J. M. Analysis of the Singlet–Triplet Splitting Computed by the Density Functional Theory–Broken-Symmetry Method: Is It an Exchange Coupling Constant? Inorg. Chem. **2011**, 50, 5577−5586. https://doi.org/10.1021/ic200198f

67. Spivak, M.; Vogiatzis, K. D.; Cramer, C. J. de Graaf, C.; Gagliardi, L. Quantum Chemical Characterization of Single Molecule Magnets Based on Uranium. J. Phys. Chem. A **2017**, 121: 1726–1733. https://doi.org/10.1021/acs.jpca.6b10933

68. Schultz, N. E.; Zhao, Y. Truhlar, D. G. Density Functionals for Inorganometallic and Organometallic Chemistry. J. Phys. Chem. A **2005**, 109, 11127−11143. https://doi.org/10.1021/jp0539223

69. Rudra, I.; Wu, Q.; Van Voorhis, T. Predicting Exchange Coupling Constants in Frustrated Molecular Magnets Using Density Functional Theory. Inorg. Chem. **2007**, 46, 10539−10548. https://doi.org/10.1021/ic700871f

70. Maurice, R.; Renault, E.; Gong, Y.; Rutkowski, P. X.; Gibson, J. K. Synthesis and Structures of Plutonyl Nitrate Complexes: Is Plutonium Heptavalent in $PuO_3(NO_3)^{2-}$? Inorg. Chem. **2015**, 54, 2367–2373. https://doi.org/10.1021/ic502969w

71. Singh, S. K.; Tibrewal, N. K.; Rajaraman. G. Density functional studies on dinuclear $\{Ni^{II}Gd^{III}\}$ and trinuclear $\{Ni^{II}Gd^{III}Ni^{II}\}$ complexes: magnetic exchange and magneto-structural maps. Dalton Trans., **2011**, 40, 10897. https://doi.org/10.1039/c1dt10600g

72. Ciofini, I.; Daul, C.A. DFT calculations of molecular magnetic properties of coordination compounds. Coord. Chem. Rev. **2003**, 187, 238–239. https://doi.org/10.1016/S0010-8545(02)00330-2

73. Yamaguchi, K.; Jensen, F.; Dorigo, A.; Houk, K.N. A spin correction procedure for unrestricted Hartree-Fock and Møller-Plesset wavefunctions for singlet diradicals and polyradicals. Chem. Phys. Lett. **1988**, 149, 537. https://doi.org/10.1016/0009-2614(88)80378-6

74. Onishi, T.; Yamaki, D.; Yamaguchi, K.; Takano, Y. Theoretical calculations of effective exchange integrals by spin projected and unprojected broken-symmetry methods. I. Cluster models of-type solids. J. Chem. Phys. **2003**, 118, 9747−9761. https://doi.org/10.1063/1.1567251

75. Shoji, M.; Koizumi, K.; Kitagawa, Y.; Kawakami, T.; Yamanaka, S.; Okumura, M.; Yamaguchi, K. A general algorithm for calculation of Heisenberg exchange integrals J in multi-spin systems. Chem. Phys. Lett. **2006**, 432, 343−347. https://doi.org/10.1016/j.cplett.2006.10.023

76. Ruiz, E.; Cano, J.; Alvarez, S.; Alemany, P. Broken Symmetry Approach to Calculation of Exchange Coupling Constants for Homobinuclear and Heterobinuclear Transition Metal Complexes. J. Comput. Chem. **1999**, 20, 1391–1400. https://doi.org/10.1002/(SICI)1096-987X(199910)20:13<1391::AID-JCC6>3.0.CO;2-J

77. Reed, A.E.; Curtiss, L. A.; Weinhold, F. Intermolecular interactions from a natural bond orbital, donor-acceptor viewpoint. Chem. Rev. **1988**, 88, 899-926. https://doi.org/10.1021/cr00088a005

78. Mayer, I. Charge, bond order and valence in the ab initio SCF theory. Chem. Phys. Lett. **1983**, 97, 270-274. https://doi.org/10.1016/0009-2614(83)80005-0

79. Nalewajski, R. F.; Mrozek, J. Modified valence indices from the two-particle density matrix. Int. J. Quantum Chem. **1994**, 51, 187-200. https://doi.org/10.1002/qua.560510403

80. Nalewajski, R.F.; Mrozek J.; Michalak, A. Two-electron valence indices from the Kohn-Sham orbitals. Int. J. Quantum Chem. **1997**, 61: 589-601. https://doi.org/10.1002/(sici)1097-461x(1997)61:3<589::aid-qua28>3.0.co;2-2

81. Mulliken, R. S. Electronic Population Analysis on LCAO-MO Molecular Wave Functions. I. J. Chem. Phys. **1955**, 23, 1833-1840. http://doi.org/10.1063/1.1740588

82. Wu, H.; Wu, Q.-Y.; Wang, C.-Z.; Lan, J.-H.; Liu, Z.-R.; Chai, Z.-F.; Shi, W.-Q. New insights into the selectivity of four 1,10-phenanthroline-derived ligands toward the separation of trivalent actinides and lanthanides: a DFT based comparison study. Dalton Trans. Int. Ed. **2016**, 45, 8107-8117. https://doi.org/10.1039/c6dt00296j

83. Kozimor, S. A.; Yang, P.; Batista, E. R.; Boland, K. S.; Burns, C. J.; Clark, D. L.; Conradson, S. D.; Martin, R. L.; Wilkerson, M. P.; Wolfsberg, L. E. J. Am. Chem. Soc. **2009**, 131, 12125−12136. https://doi.org/10.1021/ja9015759

84. Kaltsoyannis, N. Does Covalency Increase or Decrease across the Actinide Series? Implications for Minor Actinide Partitioning. Inorg. Chem. **2013**, 52, 3407. https://doi.org/10.1021/ic3006025

85. Neidig, M. L.; Clark, D. L.; Martin, R. L. Covalency in f-element complexes. Coord. Chem. Rev. **2013**, 257, 394−406. https://doi.org/10.1016/j.ccr.2012.04.029

86. Caneschi, A.; Dei, A.; Gatteschi, D.; Sorace, L.; Vostrikova, K. Antiferromagnetic Coupling in a Gadolinium(III) Semiquinonato Complex. Angew. Chem., Int. Ed. **2000**, 39, 246-248. https://doi.org/10.1002/(SICI)1521-3773(20000103)39:1<246::AID-ANIE246>3.0.CO;2-B